REVIEW ARTICLE

Dynamic Risk-Adjusted Monitoring of Time Between Events: Applications of NHPP in Pipeline Accident Surveillance

Hussam Ahmad[1] | Adel Ahmadi Nadi[2] | Mohammad Amini[3] | Subhabrata Chakraborti[4]

[1]Department of Mathematics, Faculty of Science, Al Furat University, Deir-ez-Zor, Syrian Arab Republic | [2]Department of Statistics and Actuarial Science, University of Waterloo, Waterloo, Canada | [3]Department of Statistics, Faculty of Mathematical Sciences, Ferdowsi University of Mashhad, Mashhad, Iran | [4]Department of Information Systems, Statistics and Management Science, The University of Alabama, Tuscaloosa, Alabama, USA

Correspondence: Adel Ahmadi Nadi (adel.ahmadinadi@uwaterloo.ca)

ABSTRACT

Monitoring time between events (TBE) is essential in many industrial settings. Traditional methods assume a time-invariant failure rate which is unsuitable for complex systems where the failure mechanism changes over time due to degradation. The Non-Homogeneous Poisson Process (NHPP) better models these systems by allowing a time-varying failure intensity. Additionally, failure patterns of such systems are often influenced by risk factors like environmental conditions and human interventions. Restoration of such systems also imposes multiple cost constraints. This work proposes a novel approach: a risk-adjusted control chart based on the NHPP model, specifically designed for monitoring the ratio, Cost/TBE, called the average cost per time unit. Risk-adjustment enhances the chart's detectability of shifts in the failure process by isolating the risk factors' contribution. Moreover, incorporating cost-based monitoring statistics not only emphasizes the cost impacts beside the failures themselves but also improves the chart's interpretability. The effectiveness of the proposed method is demonstrated through a comprehensive numerical study showing its superior performance compared to existing methods. The comparison study shows that ignoring the risk factors in the chart design leads to numerous false alarms, undermining the chart's effectiveness. We also illustrated the proposed method through a case study on monitoring a network of oil pipeline accidents.

1 | Introduction

An important focus of statistical process monitoring (SPM) methods is to develop efficient control charts to monitor the quality of a process over time, and to improve process performance by providing valuable insights into the process stability and the variability [1]. Though the ideas were first introduced to monitor industrial processes (e.g., a manufacturing process), they have now gained a strong foothold in many nonindustrial sectors, including medicine, healthcare and public health, surveillance, financial markets, climate and environment, chemical engineer-

ing, network monitoring, and change-point problems, see for example [2–8]. In an industrial context, SPM techniques can noticeably contribute to improving the quality of manufacturing processes by monitoring the output of the process over time. As another example, in a financial context, SPM tools can be used for various financial applications such as portfolio monitoring and stock trading [9].

One important application of SPM is in the context of monitoring defectives or failures, where attribute control charts (e.g., p chart) have been traditionally used. However, for monitoring

high-quality processes, where the number of defectives (failures) is often (most) likely to be zero, a more efficient monitoring procedure is to focus on the elapsed time between two successive defective items and not on monitoring the number of defectives. Time-between-events (TBE) control charts are widely used for this purpose. Note that in this context, although traditionally, the event of interest has been the "production of a defective item," the idea is not limited to this case, and the event of interest can include a broad range of applications, even in nonmanufacturing contexts, such as the time between disease outbreaks in a healthcare context or the time between failures of operating systems in the industrial sector. To be consistent, throughout the paper, "system" will refer to a "manufactured item," or a "production process," or a "repairable system." Likewise, a "failure or defective" will refer to any such event of interest, depending on the context.

Most of the studies on TBE charts assume that the failures occur according to a homogeneous Poisson process (HPP), which results in the TBE distribution being the well-known exponential distribution [10–13]. This means that the deterioration mechanism of an equipment, say its hazard rate function, is assumed to be constant over time. While this assumption may apply in some cases, it may not be valid, even for noncomplex production equipments, where more deterioration is expected with time. This argument could also be true in other process monitoring settings. For example, if the goal is to monitor the real-time condition of a repairable system via monitoring the time between its failures, then the HPP may not be an efficient choice. A repairable system is a system that can be repaired after breaking down; thus its failure rate is most likely to change with time and accordingly the non-homogeneous Poisson process (NHPP) is a more realistic choice to model the number of failures of such a system [14]. In practice, many systems exhibit complexities and dynamic behaviors, making it challenging to assume a constant failure rate. In such cases, the NHPP offers a more accurate representation of such systems by accounting for varying rates and capturing different failure patterns [15, 16]. That is why the NHPP plays a central role in modeling the failure counts of complex systems in reliability analysis and maintenance literature [17–21]. Despite this, the attention to NHPP has been relatively low in the SPM literature.

It is essential to recognize that any failure of a system may come with some costs to bring it back to operation. These costs may include expenses for repairs and replacements, parts and labor, downtime, warranty claims, as well as potential penalties and fines, either individually or in combination. Since the total cost (TC) associated with each failure may be affected by various factors, it makes more sense to treat it as a random quantity (variable). In the TBE literature, the "amplitude" variable is often used to represent the random variable TC. Many techniques have been developed for monitoring the TBE and the amplitude/TC variables, simultaneously, that are also known as the TBEA control charts [22–24].

Note that the failure time datasets often include information about some risk factors (also known as the covariates or confounding variables) in addition to the time to failures and their costs. These factors provide a wide range of information and can noticeably affect the performance of the system. Ignoring them

in the analysis can be costly, causing a high degree of variation and overall deterioration in the system's performance [25, 26]. There are several models in the literature to incorporate the relevant risk factor information. These include the well-known Cox proportional hazards model, which is more likely to be applied to account for system-reliability-related risk factors in an industrial context, and the accelerated failure time model, which is more commonly used to account for health-related risk factors in a clinical context [27]. Applying a proper risk model to account for the effects of the risk factors provides a more informative framework [28]. In the healthcare-related SPM domain, several control charts have been developed that account for the effect of patient's preoperative risk factors. Among the pioneering works in this area, Steiner et al. [29, 30] studied risk-adjusted control charts to track patient death rates. Since then, a huge body of risk-adjusted monitoring methods has been proposed by different scientists [31–33]. Also, Paynabar et al. [34] introduced a comprehensive phase I risk-adjusted control chart for monitoring binary surgical outcomes by considering categorical covariates. Steiner [35] provides a list of justifications for risk adjustment in the health context. For example, they stated that patients may have different conditions before treatment and thus are not expected to be homogeneous (unlike manufactured parts). One can argue the same is true in the case of monitoring the performance of systems in the presence of different risk factors such as material, labor, weather conditions, and so forth. Risk adjustment in this case takes care to distinguish the failure mechanism of the system itself from the risk model. By doing this, the monitoring method would be more sensitive to the changes of system failures and associated costs [36, 37].

Although risk-adjusted control charts have been extensively studied in healthcare, their application in SPM for industrial settings remains relatively unexplored. This paper aims to fill this gap by developing a dynamic risk-adjusted control chart for monitoring the average cost per time unit, defined as the ratio TC/TBE, using the NHPP model to account for the time-varying failure intensity. Integrating TC and risk factors directly into the control chart enhances interpretability and sensitivity, providing a more effective approach to monitoring the failure mechanisms. The rest of the paper is structured as follows: Section 2 presents a motivational example based on pipeline accident data that forms the background of this work. Section 3 briefly introduces the NHPP with two widely used intensity models, as well as discusses the risk adjustment approach. Section 4 offers an overview of the basic principles and background of copula theory. Moving on, Section 5 focuses on the construction of the proposed control chart, while Section 6 presents a numerical study that evaluates the performance of the charts. In Section 7, a practical application of the proposed charts based on real data examples is discussed. Finally, the study is concluded in Section 8 with a concise summary of the main findings and conclusions, along with suggested directions for future research.

2 | Motivational Example

The Pipeline and Hazardous Materials Safety Administration (PHMSA) of the United States Department of Transportation

has released a comprehensive report, including a dataset, on oil pipeline accidents between January 1, 2010, and September 1, 2017. The accident/failure of oil pipelines refers to an incident in which the pipeline leaks or ruptures, releasing the contents of the pipeline. Such failures can be hazardous and can potentially cause damage to the environment and human health as well as economic losses [38–41]. The financial consequences of pipeline accidents are also substantial [42]. The TC of oil spill response and cleanup operations globally ranges from tens of millions to billions of dollars annually [43]. That is why it is crucial to provide efficient strategies to inspect the pipelines, monitor their potential failures, and develop emergency response plans in case of a failure. All these kinds of efforts could be highly beneficial to minimize the risk and cost of failures, as well as to prevent any unexpected failures. By closely monitoring pipeline accidents, operators can detect potential issues at an early stage and take corrective and preventive actions before they either escalate or happen again in the future.

The database comprises details of 2781 accidents and is publicly available on the Kaggle website (https://www.kaggle.com/datasets/usdot/pipeline-accidents). Various costs (e.g., property damage costs, lost commodity costs, emergency damage costs, etc.) were incurred in order to repair the pipeline and bring it back into the network. In addition, the dataset provides the TC associated with each accident, which is the aggregate sum of all incurred costs. Furthermore, at the time of each accident, information regarding the pipeline type and location, the type of hazardous liquid involved, the accident location, and the accident cause has also been recorded. All these risk factors could potentially affect the intensity or pattern of the accidents. A number of articles on the analysis of pipeline failures show that an NHPP provides a satisfactory model for pipeline incidents, for example [44, 45]. Accordingly, an NHPP that accounts for a time-dependent accident rate and adjusts for risk factors is expected to provide a better statistical model for the accident mechanism of pipelines. In this context, there is a need to develop a monitoring technique based on a risk-adjusted NHPP model (RANHPP). Thus, the proposed monitoring approach can serve as a real-time surveillance system to detect statistically and practically significant (unusual) deviations (increases and decreases) in the times between successive accidents and the associated TC from the baseline of (expected) accident patterns. Accordingly, the proposed methodology can help in dealing with and mitigating these undesirable, and unsafe situations and managing the associated risks and costs.

In what follows, we present additional information about the dataset to provide a deeper understanding. Note that the majority of these incidents are concentrated in the central and southern regions of the United States (US). This geographical distribution of accidents across the US is depicted in Figure 1. For instance, the state of Texas has reported 1004 accidents, whereas the number of accidents is considerably lower in the northwest of the US, such as in the state of Oregon state, where only four accidents have been recorded (see Figure 2). According to Figure 2, approximately 50% of accidents occur in pipelines that are used for transporting crude oil. However, when considering the location of the pipelines, 99% of the accidents happen with onshore pipelines, with 53% of them being above ground. Additionally, about 51%

of accidents are attributed to material, welding, or equipment failures.

Figure 3a,b shows the letter-value plots for the TBE data (observations) (ranging from 0 to 250 h) and the TC data (ranging from 0 to 50 million USD). The letter-value plot provides a more accurate visualization compared to the traditional box plots for large and highly skewed data sets [46], which is indeed the case in this pipeline accidents dataset. Based on these figures, it's evident that the majority of TBE data points fall within the interval of (0, 50) h, indicating that most failures occur in close succession. Additionally, a significant portion of the TC data is concentrated in the range of zero to five million dollars, suggesting that most incidents are associated with relatively lower costs. Both these figures suggest right-skewed distributions for both TBE and TC variables while showing a small number of outliers in the dataset.

3 | Risk-Adjusted Nonhomogeneous Poisson Process

The NHPP is a counting process that allows the process failure rate/intensity to change with time. Denoting an NHPP with $N(t)$ for $t > 0$, where $N(t)$ represents the number of failures that occurred in the time interval $(0, t]$. The process $N(t)$ can be fully characterized by the intensity function $\lambda(t)$ that quantifies the failure rate at time t. The NHPP satisfies the following conditions:

- $N(0) = 0$, which means that no failures occur at time $t = 0$.
- The process has independent increments, which means that the number of failures in disjoint intervals $(s_1, s_2]$ and $(t_1, t_2]$ are independent.
- At most one failure can occur in any infinitesimal time interval, i.e., $P(N(t + \Delta t) - N(t) \geq 2) = 0$.
- The probability that a failure occurs in the time interval $[t, t + \Delta t]$ is given by $P(N(t + \Delta t) - N(t) = 1) = \lambda(t)\Delta t + o(\Delta t)$.

It follows that in an NHPP, the number of failures in the time interval $(s, t]$ follows a Poisson distribution with parameter $\Lambda(t) - \Lambda(s)$ where $\Lambda(t) = E(N(t)) = \int_0^t \lambda(u)du$ is called the mean function (also known as cumulative intensity function) of the process. Thus, we have:

$$\Pr(N(t) - N(s) = k) = \frac{(\Lambda(t) - \Lambda(s))^k}{k!} \exp(\Lambda(s)$$
$$-\Lambda(t)), k = 0, 1, 2, \dots \quad (1)$$

According to Equation (1), it can be inferred that the $N(t)$ follows a Poisson distribution with the parameter $\Lambda(t)$. When the intensity function is constant, i.e., $\lambda(t) = \gamma$, the NHPP reduces to the HPP with the constant rate γ. The intensity function $\lambda(t)$ can take different mathematical forms. However, in many applications, the log-linear and the power-law models are the most widely used. The following two subsections provide a brief introduction to these models.
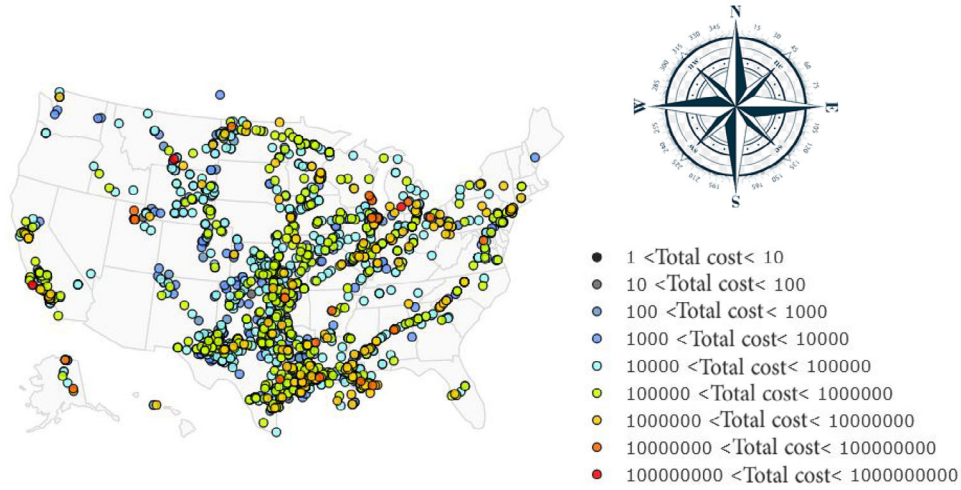
FIGURE 1 | The distribution of the accidents across the US along with TC in USD.
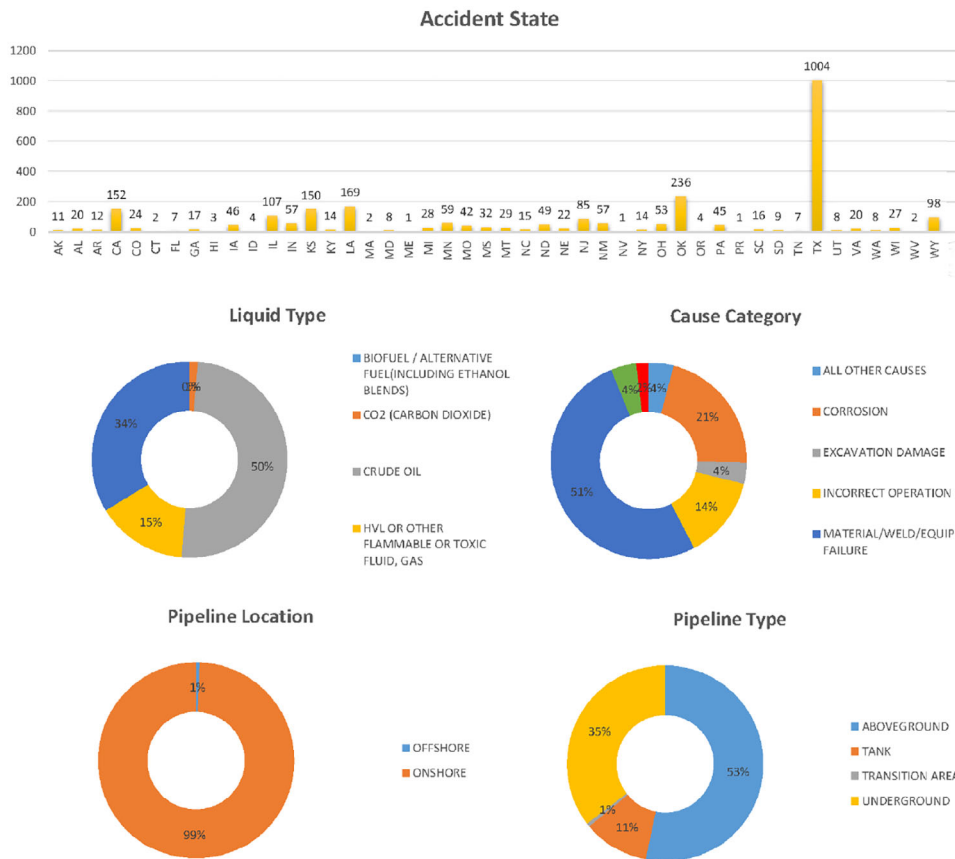
FIGURE 2 | The distribution of accidents across five risk factors.

3.1 | Power Law Intensity Model

The power law intensity function, which is also known as the Weibull model, is a widely used failure rate function in NHPP applications with the mathematical form:

$$\lambda(t) = \gamma\eta t^{\eta-1}, \tag{2}$$

and with the mean function:

$$\Lambda(t) = \int_0^t \gamma\eta u^{\eta-1} du = \gamma t^{\eta}, \tag{3}$$

where $\gamma > 0$ is the scale and $\eta > 0$ is shape parameter. According to (2), $\eta > 1$ results in a shorter time between failures, while $0 < \eta < 1$ leads to a longer TBE. If $\eta = 1$, the failure process becomes

(a) TBE (in hour).

(b) TC (in million USD).
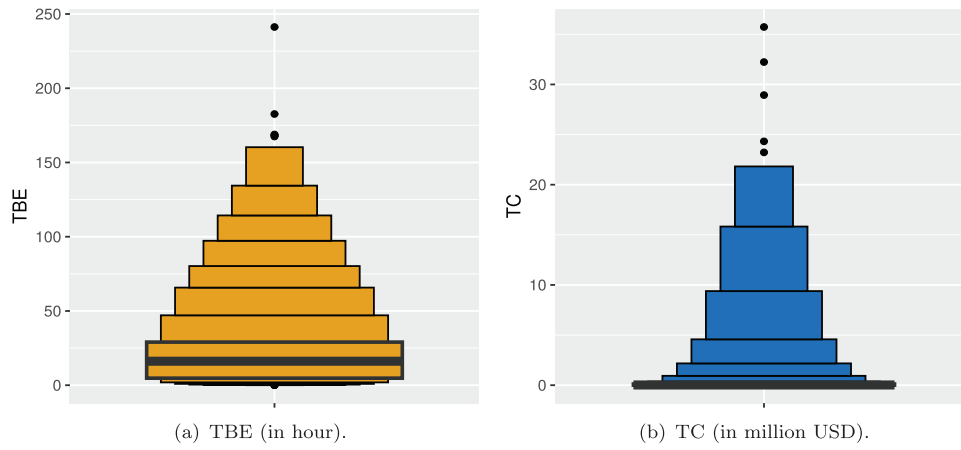
FIGURE 3 | Letter-value plots for TBE and TC.

an HPP and the TBE follows an exponential distribution with rate γ.

3.2 | Log-Linear Intensity Model

Another common way to model the intensity function of an NHPP is using a log-linear model with the following mathematical form:

$$\lambda(t) = \exp(\gamma + \eta t), \quad (4)$$

where γ and η are real constants; changes have been made here γ corresponds to the initial failure rate (at time $t = 0$) and η quantifies the magnitude of the failure rate's changes proportional to the time. The mean function corresponding to the log-linear model can be calculated as:

$$\Lambda(t) = \int_0^t \exp(\gamma + \eta u) du = \frac{1}{\eta}(\exp(\gamma + \eta t) - \exp(\gamma)). \quad (5)$$

The values of γ and η in the above setting allow for modeling a diverse range of time-dependent patterns in failure rates, including accelerating, decelerating, and constant failure rates, over time. According to (4), the value of $\eta > 0$ shows a positive association between the failure intensity and time, which results in a shorter time between failures, while a negative η leads to a longer time between failures. On the other hand, when $\eta = 0$, the failure process reduces to an HPP, and the TBE follows an exponential distribution with rate e^γ.

We conclude this subsection with a brief discussion of the power law and the log-linear intensity functions, which differ in how they model the event rates in an NHPP. A key feature of the log-linear model is that its failure intensity is strictly positive at $t = 0$ and remains convex for any value of η. This makes it particularly suitable for modeling repairable systems that exhibit a rapidly increasing failure rate. More broadly, these models represent different temporal behaviors. The power law intensity function assumes the event rate scales as a power of time, making it well-suited for systems like aging hardware or equipment where failures accelerate or decelerate over time. Conversely, the log-linear intensity function assumes that the event rate changes

exponentially with time, capturing more complex and nonlinear failure patterns. This makes it ideal for applications such as software reliability, maintainability modeling, or environmental monitoring. Ultimately, the choice between these models depends on the context, the nature of the data, specifically, whether event rates evolve gradually or sharply, and whether the pace of change is constant or dynamic.

3.3 | Risk Adjustment

Within the NHPP framework, acknowledging the impact of various risk factors on system failure mechanisms emphasizes the essential need for a model that adjusts for these risks. This section is devoted to discussing the RANHPP (risk-adjusted NHPP) model. In many real-world applications, the failure mechanism of a system can be influenced by various risk factors. For instance, in our motivating example, factors such as the pipeline type, the cause of the accident, and the type of hazardous liquid can all affect pipeline failures. When risk factors are present, a risk-adjusted model allows for a separate estimation of the intensity function from the effects of the risk factors. This leads to a more reliable estimate of the system's failure rate.

The Cox proportional hazards (PH) model is the most widely employed technique in survival studies for analyzing time-to-event data in the presence of risk factors. This model assumes that risk factors have a multiplicative influence on the hazard function, without necessitating a constant hazard function or adherence to a specific distribution. The PH model relates the hazard function at time t with the vector of risk factors $\mathbf{z}_t = (z_{t1}, z_{t2}, ..., z_{tp})$ collected at this time to a baseline hazard (intensity) function as:

$$\lambda(t|\mathbf{z}_t) = \lambda(t) \exp(\boldsymbol{\beta}' \mathbf{z}_t), \quad (6)$$

where $\boldsymbol{\beta} = (\beta_1, \beta_2, ..., \beta_p)$ is a vector of p unknown regression coefficients and $\lambda(t)$ is the baseline intensity function which only depends on time t and is given in Equations (2) and (4). The interpretation of beta values depends on the scale and nature of the risk factors. The risk-adjusted intensity function $\lambda(t|\mathbf{z}_t)$ in (6)

can be used to derive the risk-adjusted mean function as:

$$\Lambda(t|\mathbf{z}_t) = \int_0^t \lambda(u|\mathbf{z})du = \Lambda(t)\exp\left(\boldsymbol{\beta}'\mathbf{z}_t\right), \qquad (7)$$

where $\Lambda(t)$ is given in Equations (3) and (5). As per the Equation (6), the impact of risk factors on failures is quantified through the regression coefficients $\boldsymbol{\beta}$. In the presence of one risk factor ($p = 1$), a positive β value implies that $\exp(\beta z_t) > 1$, which in turn increases the expected number of failures in the time interval $(0, t]$ and thus reduces the time between failures. Conversely, negative β values suggest a decrease in the expected number of failures resulting in a longer time between failures. In the upcoming section, we will delve into the dependence among variables.

4 | Dependence Modeling

Dependence among the variables is an important factor in practical applications. Copula modeling has emerged as a widely adopted technique for capturing dependencies in various domains of application. It offers the ability to disentangle the dependence structure from the joint distribution function of a set of variables while preserving their individual univariate marginals. Sklar's theorem plays a pivotal role in this process, allowing us to establish the joint distribution $H(x, y)$ of two random variables, namely X and Y, with marginal CDF $F_X(.|\boldsymbol{\theta}_X)$ and $F_Y(.|\boldsymbol{\theta}_Y)$, respectively. The equation for $H(x, y|\boldsymbol{\theta}_X, \boldsymbol{\theta}_Y, C)$ involves the copula model C once its parametric form is determined, where:

$$H(x, y|\boldsymbol{\theta}_X, \boldsymbol{\theta}_Y, C) = C(F_X(x|\boldsymbol{\theta}_X), F_Y(y|\boldsymbol{\theta}_Y)|\theta_c), \qquad (8)$$

where $\boldsymbol{\theta}_X$ ($\boldsymbol{\theta}_Y$) is the vector of X (Y) distribution's parameters and θ_c is the parameter of the copula function C. A key advantage of Sklar's theorem lies in its guarantee that a unique copula C exists when dealing with continuous marginal distributions, as is the case in our study. Before delving into specific copula models, it is essential to introduce the dependence measure known as Kendall's tau τ.

4.1 | Kendall's Tau τ

Kendall's tau $\tau \in [-1, 1]$ is a widely used metric for quantifying dependencies and associations between two random variables. For continuous random variables X and Y with a copula C, Kendall's tau is defined specifically in terms of cumulative distribution functions (CDFs). This approach highlights the nonparametric nature of Kendall's tau and its independence from specific distributional assumptions. Kendall's tau τ can be computed using the formula:

$$\tau = 4 \iint_{[0,1]^2} C(u, v)\mathrm{d}C(u, v) - 1. \qquad (9)$$

Here, $C(u, v)$ represents the joint CDF of the transformed random variables $U = F_X(X)$ and $V = F_Y(Y)$, where X and Y are continuous random variables with marginal CDFs $F_X(x)$ and $F_Y(y)$, respectively. According to the probability integral transform [47],

the variables U and V each follows the standard uniform distribution. The coefficient τ in (9) measures the associations between two variables. Values $\tau \in (0, 1)$ indicate a positive association between X and Y (both variables increase/decrease together), while a $\tau \in (-1, 0)$ expresses a negative association (as one variable increases, the other one decreases). On the other hand, $\tau = 1 (\tau = -1)$ shows a perfect positive (negative) association and $\tau = 0$ indicates no association between the variables. It is also interesting to note that the integral in (9) represents the expected value of the random variable $C(U, V)$, where individual variables U and V follow a standard uniform distribution, i.e., $\tau = 4\mathbb{E}(C(U, V)) - 1$. Indeed, there exists a diverse range of copula functions with varying properties. In the subsequent subsection, we introduce the Gumbel copula from Archimedean family and highlight its distinctive characteristics.

4.2 | Gumbel Copula Model

There could be different dependence structures between the TBE and TC variables that we aim to monitor jointly over time. Castagliola et al. [12] presented examples in which there is a positive or negative or even a lack of association between TBE and TC variables. However, in the case study, they discussed that there is a strong positive association, which is equivalent to saying that the TC becomes smaller as the TBE becomes shorter. This is also more likely to happen in our case study of monitoring pipeline accidents. Accordingly, this paper focuses on the Gumbel model, which belongs to the well-known bivariate Archimedean family of copulas. The Gumbel family can represent only independence and positive dependence, as its dependence parameter is bounded between the independence copula and the Frechet-Hoeffding upper bound copula. It exhibits strong upper tail dependence and relatively weak lower tail dependence. However, the application of the proposed method is not restricted to this choice, and other copula functions that are able to model various kinds of dependency can be easily used.

The Gumbel copula, also known as the Gumbel–Hougaard model, was introduced by Gumbel [48]. Mathematically, the Gumbel copula is expressed as:

$$C(u, v) = \exp\left(-\left((-\ln(u))^{\theta_c} + (-\ln(v))^{\theta_c}\right)^{\frac{1}{\theta_c}}\right), \qquad (10)$$

where the dependence parameter θ_c is confined to the interval $[1, \infty)$. The relationship between Kendall's tau τ and the Gumbel copula parameter θ_c is given by:

$$\tau = \frac{\theta_c - 1}{\theta_c} \iff \theta_c = \frac{1}{1 - \tau}, \qquad (11)$$

where the Gumbel copula parameter (θ_c) is utilized within the copula function (Equation 11), whereas Kendall's tau (τ) is employed to characterize the dependence in numerical analysis in Section 6.
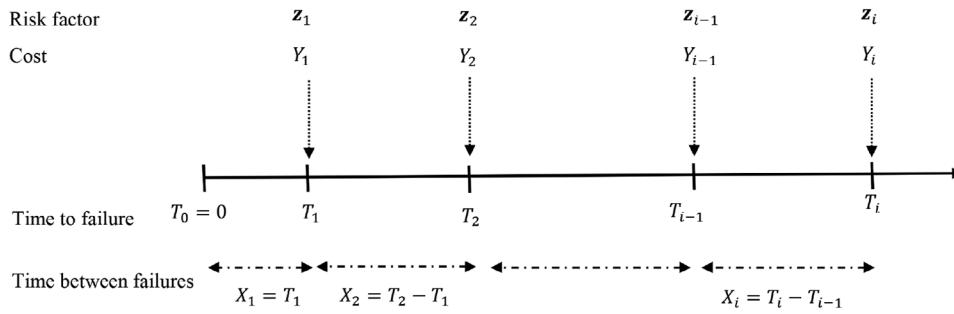
FIGURE 4 | Data collection schematic.

5 | Proposed Dynamic Monitoring Technique

Recall that the main aim of this work is to develop a control chart to monitor the TBE variable and its associated TC, while accounting for the risk factors recorded at the time of each failure. In this setting, one reasonable quantity for monitoring the stability of such a process, that incorporates the effects of these two factors, is the average cost per unit time (AC), so that AC = TC/TBE. The average cost per unit time metric also has a meaningful interpretation, making the control chart more practically meaningful and providing valuable insights into the financial implications. Both of these are relevant aspects of the decision-making process.

We assume that the system starts to operate at time $T_0 = 0$. As time passes, failures may occur at random times $T_1, T_2, \ldots$ resulting in TBEs $X_1 = T_1, X_2 = T_2 - T_1, \ldots$. In addition, at time t_i of failure $i = 1, 2, \ldots$, data on the risk factors and the TC variable denoted by $z_{i1}, \ldots, z_{ip}$ and Y_i, respectively, are collected. Figure 4 shows a schematic of this data collection process.

To calculate the control limits of the proposed monitoring scheme, we first derive the conditional CDF of the ith failure time T_i given the vector of risk factors z_i and the fact that $T_{i-1} = t_{i-1}$ as:

$$P(T_i \leq t_i | T_{i-1} = t_{i-1}, z_i, \theta_X) = 1 - P(N(t_i) - N(T_{i-1}) = 0 | T_{i-1} = t_{i-1})$$
$$= 1 - P(N(t_i) - N(t_{i-1}) = 0)$$
$$= 1 - \exp(-\Lambda(t_i | z_i) + \Lambda(t_{i-1} | z_i)), \quad (12)$$

where $\theta_X = (\gamma, \eta, \beta)$ is the vector of parameters regarding the intensity function and risk model and $\Lambda(. | z_i)$ is given in (7). The second equality in (12) is obtained using the independent increments of NHPP and the third one is obtained using the fact that:

$$P(N(t_{i-1} + x) - N(t_{i-1}) = k | T_{i-1} = t_{i-1}, z_i, \theta_X)$$
$$= \frac{[\Lambda(t_{i-1} + x | z_i) - \Lambda(t_{i-1} | z_i)]^k}{k!} e^{-[\Lambda(t_{i-1} + x | z_i) - \Lambda(t_{i-1} | z_i)]}. \quad (13)$$

Eventually, the conditional CDF of X_i given $T_{i-1} = t_{i-1}$ and z_i can be obtained using Equation (12) as follows:

$$P(X_i \leq x | T_{i-1} = t_{i-1}, z_i, \theta_X)$$
$$= 1 - \exp(-\Lambda(t_{i-1} + x | z_i) + \Lambda(t_{i-1} | z_i)). \quad (14)$$

As a result, the conditional probability density function (PDF) of X_i can be calculated as:

$$f_{(X_i | t_{i-1}, z_i)}(x | \theta_X) = \lambda(t_{i-1} + x | z_i)$$
$$\exp(-\Lambda(t_{i-1} + x | z_i) + \Lambda(t_{i-1} | z_i)). \quad (15)$$

Let Y_i be the corresponding random TC of failure $i = 1, 2, \ldots$ having the CDF $F_{Y_i}(.)$ and PDF $f_{Y_i}(.)$ with the vector of parameters θ_Y. Furthermore, let us assume X_i and Y_i to be dependent and their joint CDF is given by:

$$F_{(X_i, Y_i | t_{i-1}, z_i)}(x, y | \theta) = C(F_{(X_i | t_{i-1}, z_i)}(x | \theta_X), F_{Y_i}(y | \theta_Y) | \theta_c), \quad (16)$$

where $C(u, v | \theta_c)$ is a Copula model containing all information on the dependence structure between Y_i and X_i and $\theta = (\theta_X, \theta_Y, \theta_c)$. Accordingly, the joint PDF of Y_i and X_i can be derived as:

$$f_{(X_i, Y_i | t_{i-1}, z_i)}(x, y | \theta) = f_{(X_i | t_{i-1}, z_i)}(x | \theta_X) . f_{Y_i}(y | \theta_Y) \times$$
$$c(F_{(X_i | t_{i-1}, z_i)}(x | \theta_X), F_{Y_i}(y | \theta_Y) | \theta_c), \quad (17)$$

where $f_{(X_i | t_{i-1}, z_i)}(. | \theta_X)$ is given in (15), $f_{Y_i}(. | \theta_Y)$ is the PDF of Y_i, and $c(u, v | \theta_c) = \frac{\partial C(u, v | \theta_c)}{\partial u \partial v}$ is the copula density.

5.1 | The Monitoring Statistic

According to the background provided in the previous subsection, the average cost per time unit, at the time of failure, i can be defined by $AC = E\left(\frac{Y_i}{X_i}\right)$ and be calculated as:

$$E\left(\frac{Y_i}{X_i} | t_{i-1}, z_i, \theta\right) = \int_0^\infty \int_0^\infty \frac{y_i}{x_i} f_{(X_i, Y_i | t_{i-1}, z_i, \theta)}(x, y) dy_i dx_i, \quad (18)$$

where $f_{(X_i, Y_i | t_{i-1}, z_i, \theta)}$ is given in (17). By the definition, a small value of AC is typically desired as it indicates lower average costs incurred per failure. We propose to calculate the following

ALGORITHM 1 | ARL and SDRL calculation algorithm.

Input : $\alpha, \gamma, \eta, \mu, \theta_c, \beta, \tau$.
Output: ARL, SDRL
RL ← (...)   ▷ Initialize the vector to store RL values
for *i=1 to large number* **do**
    j ← 1; t_0 ← 0;   ▷ Time to start ($t_0 = 0$).
    repeat
        for *k=1 to 10,000* **do**
            z_k ← sample({1, 2, 3}, size = 1, replace = *TRUE*, prob = dpois({1, 2, 3}, 1));
            $(U_k, V_k) \sim C(U, V | \theta_c)$;
            $Xs_k \leftarrow F_X^{-1}(U_k | t_{k-1}, \mathbf{z}_k, \theta_X), Ys_k \leftarrow F_Y^{-1}(V_k | \mu)$;
            $Ws_k \leftarrow \frac{Ys_k}{Xs_k}$;
        end
        $UCL_j \leftarrow Quantile(Ws, 1 - \frac{\alpha}{2})$;
        $LCL_j \leftarrow Quantile(Ws, \frac{\alpha}{2})$;
        $(U, V) \sim C(U, V | \theta_c)$;   ▷ For next failure;
        z_j ← sample({1, 2, 3}, size = 1, replace = *TRUE*, prob = dpois({1, 2, 3}, 1));
        $X_j \leftarrow F_{X_j}^{-1}(U | t_{j-1}, \mathbf{z}_j, \theta_X), Y_j \leftarrow F_Y^{-1}(V | \mu), W_j \leftarrow \frac{Y_j}{X_j}$;
        $t_j \leftarrow t_{j-1} + X_j$;
        j ← j+1;
    until $W_j > UCL_j$ *or* $W_j < LCL_j$;
    RL[i] ← j;
end
ARL ← E(RL); SDRL ← SD(RL)

---

monitoring statistic at the time of failure *i*:

$$W_i = \frac{Y_i}{X_i}, \qquad \text{for} \qquad i = 1, 2, \dots, \qquad (19)$$

with the aim of detecting possible deviations of the AC from its in-control (IC) state to an out-of-control (OC) state as quickly as possible. Let θ_0 and θ_1 denote the vectors of IC and OC parameters. Accordingly, monitoring the AC over time could be done by developing a proper control chart for the sequence of W_i. The proposed monitor statistic W_i further satisfies the following properties:

1. W_i decreases with X_i and increases with Y_i.

2. W_i increases with X_i and decreases with Y_i.

Let $F_{W_i}(. | t_{i-1}, \mathbf{z}_i, \theta)$ be the conditional CDF of W_i given $t_{i-1}, \mathbf{z}_i$ and θ. Then, it can be calculated as follows:

$$\begin{aligned} F_{W_i}(w | t_{i-1}, \mathbf{z}_i, \theta) &= P(W_i \le w | t_{i-1}, \mathbf{z}_i, \theta) \\ &= P\left(\frac{Y_i}{X_i} \le w | t_{i-1}, \mathbf{z}_i, \theta\right) \\ &= \int_0^\infty \int_0^{xw} f_{(X_i, Y_i | t_{i-1}, \mathbf{z}_i)}(x, y | \theta) dy dx, \quad (20) \end{aligned}$$

where $f_{(X_i, Y_i | t_{i-1}, \mathbf{z}_i)}(., . | \theta)$ is given in (17).

While a higher shift in the AC may be more of interest to detect from a financial point of view, detecting lower shifts can be valuable in assessing any improvements made to the process. Therefore, we propose implementing a two-sided control chart

capable of detecting changes in the AC that may occur in either direction, above or below the IC value. The probability-type control limits for the proposed chart at the time of failure $i = 1, 2, \dots$ can be calculated as:

$$\begin{aligned} LCL_i &= F_{W_i}^{-1}\left(\frac{\alpha}{2} \mid t_{i-1}, \mathbf{z}_i, \theta_0\right), \\ UCL_i &= F_{W_i}^{-1}\left(1 - \frac{\alpha}{2} \mid t_{i-1}, \mathbf{z}_i, \theta_0\right), \quad (21) \end{aligned}$$

where α is the probability of a type I error (also known as false alarm rate) and $F_{W_i}^{-1}(\dots | t_{i-1}, \mathbf{z}_i, \theta_0)$ is the inverse of the CDF of W_i given in (20). Thus the control limits can be obtained by solving equations $F_{W_i}(w | t_{i-1}, \mathbf{z}_i, \theta_0) = \frac{\alpha}{2}$ and $F_{W_i}(w | t_{i-1}, \mathbf{z}_i, \theta_0) = 1 - \frac{\alpha}{2}$ for w numerically. Note that the index i of LCL_i and UCL_i in (21) shows that they are step-wise limits and should be calculated at the time of each failure based on the information from the previous failure (t_{i-1}) and current failure ($\mathbf{z}_i$) as well as the IC vector θ_0. Thus, at the time of failure $i = 1, 2, \dots$, one needs to first calculate the control limits and then compare W_i with them; if $W_i > UCL_i$ or $W_i < LCL_i$, the control chart triggers an OC signal, if not, process monitoring continues.

The average run length (ARL) is one of the most popular measures to assess the performance of a control chart and to compare it with alternative charts (see Gibbons and Chakraborti [49]). ARL is the expected value of Run Length (RL), defined as the average number of samples taken before the first OC signal (the monitoring statistic falls beyond the control limits). When the successive monitoring statistics are independent, the IC RL (RL_0) follows a Geometric distribution with probability α where α is the probability of a false alarm, that is, when an IC process is diagnosed as OC by the control chart. In this case, we have

TABLE 1 | The ARL (SDRL) values based on power law intensity for $\beta = -2.00, -0.50$ with $\gamma_0 = 0.05$, $\eta_0 = 1.50$, $\mu_0 = 1.00$ when $\tau = 0.3$ (upper block) and $\tau = 0.8$ (lower block).

$(\delta_\gamma, \delta_\eta), \delta_\mu$	$\beta = -2.00$					$\beta = -0.50$				
	0.25	0.75	1.00	1.25	2.00	0.25	0.75	1.00	1.25	2.00
(0.25,0.25)	1.3(0.2)	1.2(0.7)	1.2(0.8)	1.1(0.8)	1.1(0.9)	1.9(0.3)	1.7(0.3)	1.7(0.3)	1.6(0.2)	1.5(0.2)
(0.75,0.25)	1.7(0.3)	1.5(0.3)	1.5(0.3)	1.5(0.2)	1.4(0.2)	3.0(0.6)	2.7(0.6)	2.6(0.6)	2.5(0.5)	2.4(0.5)
(1.00,1.00)	80.9(79.2)	180.8(180.0)	198.9(197.9)	181.3(180.6)	152.7(150.3)	83.0(80.6)	188.7(186.1)	196.2(190.8)	195.1(194.4)	143.7(141.5)
(1.25,0.25)	1.9(1.4)	1.7(1.4)	1.7(1.5)	1.7(1.4)	1.6(1.6)	3.7(2.6)	3.3(2.9)	3.2(2.7)	3.2(2.8)	3.0(2.0)
(2.00,0.25)	2.2(1.8)	2.0(1.6)	2.0(1.1)	1.9(1.2)	1.9(0.9)	4.6(2.8)	4.2(3.1)	4.0(3.5)	4.0(3.7)	3.8(2.9)
(0.25,0.75)	19.7(18.3)	9.3(7.5)	7.7(7.3)	6.8(6.1)	5.2(4.6)	41.1(39.9)	18.5(16.9)	14.6(13.5)	12.2(10.3)	9.2(8.5)
(0.75,0.75)	55.7(55.3)	25.9(24.0)	20.9(19.8)	18.0(17.6)	12.8(10.9)	114.7(114.2)	55.3(54.5)	44.4(43.6)	37.7(36.2)	26.1(25.0)
(1.25,0.75)	88.6(87.7)	41.7(39.7)	33.5(32.5)	28.4(26.8)	20.7(20.4)	149.6(147.8)	91.5(90.4)	70.3(69.7)	61.4(59.8)	44.5(43.5)
(2.00,0.75)	128.3(126.5)	64.1(63.2)	53.1(52.2)	44.8(43.4)	32.2(30.2)	160.2(159.7)	127.1(126.0)	108.9(107.6)	93.0(91.1)	69.6(68.4)
(0.25,1.25)	47.1(45.6)	110.3(109.8)	138.0(137.5)	159.6(158.4)	179.3(178.5)	81.2(80.8)	163.3(162.0)	180.4(179.4)	186.3(184.5)	159.5(157.9)
(0.75,1.25)	22.1(20.4)	58.1(56.3)	70.7(70.0)	90.7(89.4)	120.7(118.9)	38.5(37.1)	93.4(92.4)	118.4(117.5)	138.4(136.4)	169.9(168.9)
(1.25,1.25)	15.7(14.3)	40.9(39.9)	51.6(51.1)	60.1(58.6)	91.7(90.5)	26.7(25.1)	68.3(67.1)	87.9(86.6)	104.7(104.2)	144.4(143.4)
(2.00,1.25)	11.6(10.7)	29.7(27.9)	37.1(35.2)	44.2(42.8)	67.3(67.0)	19.6(18.4)	50.7(50.4)	63.1(62.6)	75.9(74.0)	108.4(108.0)
(0.25,2.00)	6.7(6.1)	13.4(12.8)	16.2(15.5)	18.4(17.9)	24.5(23.9)	17.1(16.4)	35.0(34.1)	43.8(42.7)	50.2(49.3)	68.3(67.0)
(0.75,2.00)	4.8(4.2)	9.5(8.9)	11.4(10.8)	12.9(12.4)	17.3(16.8)	12.0(11.5)	24.8(23.9)	29.7(28.4)	35.1(33.7)	47.8(46.5)
(1.25,2.00)	4.2(3.9)	8.2(7.8)	9.8(9.3)	11.4(10.9)	15.1(14.6)	10.1(9.7)	21.1(20.6)	25.8(25.0)	29.4(28.7)	39.8(39.0)
(2.00,2.00)	3.7(3.3)	7.2(6.8)	8.5(8.1)	9.8(9.4)	12.5(12.0)	8.8(8.3)	18.1(17.6)	21.7(21.0)	24.9(24.1)	34.4(33.6)
(0.25,0.25)	1.1(1.0)	1.0(0.9)	1.0(0.9)	1.0(0.9)	1.0(0.9)	1.4(1.3)	1.3(1.2)	1.3(1.2)	1.2(1.1)	1.2(1.1)
(0.75,0.25)	1.3(1.2)	1.2(1.1)	1.2(1.1)	1.2(1.1)	1.1(1.0)	1.8(1.7)	1.8(1.7)	1.7(1.6)	1.7(1.6)	1.6(1.5)
(1.00,1.00)	5.5(5.3)	159.4(158.0)	197.9(196.5)	171.2(169.8)	95.7(94.8)	6.0(5.8)	161.9(160.5)	195.0(193.6)	174.3(172.9)	94.5(93.6)
(1.25,0.25)	1.5(1.4)	1.4(1.3)	1.3(1.2)	1.3(1.2)	1.2(1.1)	1.7(1.6)	1.9(1.8)	1.9(1.8)	1.9(1.8)	1.9(1.8)
(2.00,0.25)	1.5(1.4)	1.5(1.4)	1.5(1.4)	1.4(1.3)	1.4(1.3)	1.4(1.3)	1.8(1.7)	1.8(1.7)	1.9(1.8)	2.0(1.9)
(0.25,0.75)	4.2(4.0)	2.4(2.3)	2.2(2.1)	2.0(1.9)	1.8(1.7)	10.9(10.7)	3.2(3.1)	2.7(2.6)	2.4(2.3)	2.1(2.0)
(0.75,0.75)	17.6(17.4)	5.8(5.6)	4.4(4.3)	3.7(3.6)	2.8(2.7)	38.1(37.9)	18.1(17.9)	12.3(12.1)	9.3(9.1)	5.1(5.0)
(1.25,0.75)	23.8(23.6)	12.0(11.8)	8.5(8.3)	6.7(6.5)	4.4(4.3)	21.5(21.3)	41.4(41.2)	28.7(28.5)	22.3(22.1)	11.8(11.6)
(2.00,0.75)	22.9(22.7)	24.3(24.1)	17.7(17.5)	13.9(13.7)	7.8(7.6)	3.0(2.8)	70.4(70.2)	59.6(59.4)	47.5(47.3)	26.9(26.7)

(Continues)

TABLE 1 | (Continued)

$(\delta_\gamma, \delta_\eta), \delta_\mu$	$\beta = -2.00$					$\beta = -0.50$				
	0.25	0.75	1.00	1.25	2.00	0.25	0.75	1.00	1.25	2.00
(0.25,1.25)	6.3 (6.1)	56.8 (56.6)	86.9 (86.7)	107.3 (107.1)	155.1 (154.9)	23.6 (23.4)	128.5 (128.3)	158.1 (157.9)	164.9 (164.7)	95.2 (95.0)
(0.75,1.25)	1.5 (1.4)	14.3 (14.1)	23.8 (23.6)	35.0 (34.8)	67.1 (66.9)	3.1 (2.9)	41.3 (41.1)	61.7 (61.5)	82.2 (82.0)	144.5 (144.3)
(1.25,1.25)	1.2 (1.1)	6.0 (5.8)	11.9 (11.7)	17.9 (17.7)	37.7 (37.5)	1.6 (1.4)	20.4 (20.2)	34.7 (34.5)	49.5 (49.3)	92.1 (91.9)
(2.00,1.25)	11.6(10.7)	29.7(27.9)	37.1(35.2)	44.2(42.8)	67.3(67.0)	19.6(18.4)	50.7(50.4)	63.1(62.6)	75.9(74.0)	108.4(108.0)
(0.25,2.00)	1.4 (1.3)	2.8 (2.7)	3.6 (3.5)	4.4 (4.3)	6.7 (6.6)	2.5 (2.3)	10.3 (10.1)	14.3 (14.1)	17.7 (17.5)	29.5 (29.3)
(0.75,2.00)	1.2 (1.1)	1.9 (1.8)	2.4 (2.3)	2.9 (2.8)	4.2 (4.1)	1.6 (1.5)	5.4 (5.2)	7.7 (7.5)	9.9 (9.7)	16.6 (16.4)
(1.25,2.00)	1.1 (1.0)	1.7 (1.6)	2.0 (1.9)	2.4 (2.3)	3.5 (3.4)	1.4 (1.3)	3.9 (3.7)	5.6 (5.4)	7.4 (7.2)	12.6 (12.4)
(2.00,2.00)	1.1 (1.0)	1.5 (1.4)	1.8 (1.7)	2.1 (2.0)	2.9 (2.8)	1.3 (1.2)	3.1 (2.9)	4.3 (4.1)	5.7 (5.5)	9.6 (9.4)

$\mathrm{ARL}_0 = \frac{1}{\alpha}$. It is shown that in (22) the IC RL (RL_0) of the proposed control chart is also distributed as a Geometric random variable. We have, when the process is in the IC state,

$$
\begin{aligned}
P(\mathrm{RL}_0 > n) &= P\left(\bigcap_{i=1}^{n} \{LCL_i < W_i < UCL_i\} \right) \\
&= \prod_{i=1}^{n} P(LCL_i < W_i < UCL_i \mid t_{i-1}, \boldsymbol{z_i}, \boldsymbol{\theta}_0) \\
&= \prod_{i=1}^{n} (1 - \alpha) \\
&= (1 - \alpha)^n, \quad\quad (22)
\end{aligned}
$$

where the second equality is obtained due to the independence between W_i for $i = 1, 2, ...$, which follows from the independent-increments feature of the NHPP. The OC ARL (ARL_1) of the proposed chart can be calculated using the Monte-Carlo approach, which is described in Algorithm 1 in Section 6. The standard deviation of the run length (SDRL) is another widely used metric for evaluating the performance of a control chart. Algorithm 1 in Section 6 outlines the procedure for computing both IC and OC SDRL values, denoted by SDRL_0 and SDRL_1 hereafter, using Monte Carlo simulations in the current setting.

6 | Numerical Analysis

In order to assess the performance of the proposed control chart and investigate its sensitivity with respect to various factors, this section aims to conduct a numerical study based on the ARL and SDRL metrics. First, let us set $\mathrm{ARL}_0 = 200$. In addition, consider a system where its failures come from an NHPP with power law or log-linear intensity function. The IC parameters are assumed to be $\eta_0 = 1.50$ for the power law model, $\eta_0 = 2.00$ for the log-linear model, and $\gamma_0 = 0.05$. These choices of intensity parameters represent increasing failure rates, a scenario more probable in deteriorating systems. Furthermore, we assume the associated TC represented by Y follows an Exponential distribution with IC rate $\mu_0 = 1.00$. The joint distribution of Y and X is also characterized by a Gumbel copula model. Furthermore, we introduce a single risk factor z ($p = 1$), which impacts the TBE. The risk factor will be a factor ranging from 1 to 3, generated using a truncated Poisson distribution with rate 1, which means the numbers 1, 2, and 3 will be generated with probabilities 0.36, 0.18 and 0.06, respectively. In addition, the regression coefficient β takes values from the set $\{-2.00, -0.50, 0.00, 0.50, 2.00\}$ to cover different association levels between the risk factor and TBE. To capture different levels of dependence between the TBE and the TC when they are positively associated, we consider the dependence parameter τ from the set $\{0.3, 0.8\}$. This will enable us to explore moderate and strong positive dependencies.

To conduct the numerical analysis, we assume the parameters γ and η regarding the TBE variable and the parameter μ of the TC variable are subject to shift, while β and θ_c/τ are assumed to remain unchanged. Let us donete the vector of IC parameters by

TABLE 2 | The ARL (SDRL) values based on power law intensity for $\beta = 0.50, 2.00$ with $\gamma_0 = 0.05, \eta_0 = 1.50, \mu_0 = 1.00$ when $\tau = 0.3$ (upper block) and $\tau = 0.8$ (lower block).

$(\delta_\gamma, \delta_\eta), \delta_\mu$	$\beta = 0.50$					$\beta = 2.00$				
	0.25	0.75	1.00	1.25	2.00	0.25	0.75	1.00	1.25	2.00
(0.25,0.25)	2.9(0.5)	2.7(0.5)	2.6(0.4)	2.6(0.5)	2.4(0.4)	4.1(1.1)	4.0(1.2)	3.9(1.2)	3.8(1.0)	3.9(1.0)
(0.75,0.25)	4.8(1.2)	4.5(1.2)	4.4(1.3)	4.2(1.3)	4.2(1.4)	3.5(4.0)	4.7(4.2)	5.1(4.3)	5.0(4.0)	5.1(5.0)
(1.00,1.00)	82.8(80.6)	174.1(173.8)	198.6(195.5)	187.6(186.1)	148.1(147.5)	83.6(83.2)	178.9(175.7)	197.7(196.4)	176.2(175.3)	143.8(141.7)
(1.25,0.25)	5.1(4.7)	5.3(4.9)	5.3(4.8)	5.4(4.2)	5.2(4.7)	1.9(0.8)	3.3(2.6)	3.7(2.8)	4.2(3.7)	4.8(3.4)
(2.00,0.25)	4.2(2.8)	5.6(4.7)	5.9(5.1)	6.0(5.3)	6.1(5.3)	1.1(0.7)	1.7(0.9)	2.0(1.3)	2.3(1.5)	3.3(2.7)
(0.25,0.75)	59.2(58.4)	26.1(24.7)	21.8(20.2)	18.3(16.9)	12.7(11.0)	86.7(85.9)	40.7(40.3)	33.0(32.1)	27.6(26.6)	19.4(18.9)
(0.75,0.75)	147.2(146.9)	76.3(74.6)	62.9(61.8)	53.0(52.3)	38.2(36.8)	152.0(150.8)	111.1(110.8)	91.4(89.5)	80.4(79.0)	57.4(56.2)
(1.25,0.75)	155.5(154.5)	124.2(122.6)	98.1(96.6)	91.7(90.8)	63.8(62.4)	97.3(96.3)	152.3(151.0)	134.4(132.7)	121.9(121.0)	93.5(92.0)
(2.00,0.75)	103.8(101.8)	163.2(162.7)	143.0(142.5)	128.8(127.4)	97.7(96.8)	44.1(43.1)	154.7(154.1)	162.4(161.5)	157.9(157.4)	130.3(128.8)
(0.25,1.25)	99.0(98.0)	181.0(180.3)	180.3(178.6)	172.6(171.1)	134.0(132.1)	129.4(129.1)	174.0(172.5)	158.6(156.7)	140.1(138.5)	82.5(80.9)
(0.75,1.25)	49.6(48.9)	116.6(115.4)	144.1(142.6)	159.3(158.6)	187.7(186.2)	64.0(62.7)	143.0(142.5)	168.1(166.9)	181.4(180.5)	169.1(167.3)
(1.25,1.25)	35.6(34.5)	88.6(87.8)	108.7(108.2)	123.8(122.0)	167.9(166.5)	45.6(43.8)	105.5(105.2)	134.1(133.1)	147.8(146.7)	182.5(181.0)
(2.00,1.25)	25.2(23.6)	64.2(63.8)	81.2(79.9)	97.0(95.3)	132.0(130.2)	32.9(32.2)	80.2(78.5)	103.8(102.4)	123.3(122.8)	160.8(159.8)
(0.25,2.00)	28.4(27.5)	60.1(59.2)	70.3(69.4)	79.1(77.8)	106.9(105.2)	49.8(48.9)	96.5(95.1)	112.4(111.1)	121.7(120.0)	139.7(138.5)
(0.75,2.00)	19.7(18.8)	41.5(40.2)	49.2(48.3)	56.5(55.0)	75.7(74.0)	34.5(33.7)	71.6(70.2)	82.8(81.5)	97.0(95.4)	116.4(114.8)
(1.25,2.00)	16.5(15.8)	33.9(33.1)	41.9(40.5)	48.4(47.0)	66.1(65.0)	29.0(28.1)	60.6(59.4)	71.4(70.2)	83.7(82.3)	107.2(106.0)
(2.00,2.00)	14.2(13.7)	30.4(29.6)	35.8(34.9)	41.5(40.7)	57.4(56.0)	24.8(23.9)	52.7(51.4)	64.2(62.9)	69.0(68.0)	92.2(90.5)
(0.25,0.25)	1.8(1.7)	1.8(1.7)	1.7(1.6)	1.7(1.6)	1.6(1.5)	1.3(1.2)	1.6(1.5)	1.6(1.5)	1.6(1.5)	1.7(1.6)
(0.75,0.25)	1.3(1.2)	1.7(1.6)	1.8(1.7)	1.8(1.7)	1.9(1.8)	1.0(0.9)	1.0(0.9)	1.1(1.0)	1.1(1.0)	1.2(1.1)
(1.00,1.00)	6.3(6.1)	156.8(155.4)	198.8(197.4)	178.5(177.1)	93.2(92.3)	5.6(5.4)	158.3(156.9)	201.5(200.1)	176.5(175.1)	86.3(85.4)
(1.25,0.25)	1.1(1.0)	1.3(1.2)	1.4(1.3)	1.5(1.4)	1.6(1.5)	1.3(1.2)	1.0(0.9)	1.0(0.9)	1.0(0.9)	1.0(0.9)
(2.00,0.25)	1.0(0.9)	1.1(1.0)	1.1(1.0)	1.1(1.0)	1.3(1.2)	1.1(1.0)	1.7(1.6)	1.1(1.0)	1.0(0.9)	1.0(0.9)
(0.25,0.75)	20.5(20.3)	5.2(5.1)	3.9(3.8)	3.2(3.1)	2.4(2.3)	30.0(29.8)	10.6(10.4)	7.3(7.1)	5.8(5.6)	3.6(3.5)
(0.75,0.75)	25.5(25.3)	33.3(33.1)	23.6(23.4)	17.7(17.5)	9.6(9.5)	7.6(7.4)	48.8(48.6)	42.6(42.4)	34.6(34.4)	19.6(19.4)
(1.25,0.75)	4.1(3.9)	66.5(66.3)	52.7(52.5)	41.9(41.7)	23.4(23.2)	1.0(0.9)	46.2(46.0)	60.8(60.6)	63.1(62.9)	44.0(43.8)

(Continues)

TABLE 2 | (Continued)

$(\delta_\gamma, \delta_\eta), \delta_\mu$	$\beta = 0.50$					$\beta = 2.00$				
	0.25	0.75	1.00	1.25	2.00	0.25	0.75	1.00	1.25	2.00
(2.00,0.75)	1.0 (0.9)	52.4 (52.2)	74.5 (74.3)	78.2 (78.0)	50.3 (50.1)	1.0 (0.9)	8.9 (8.7)	31.3 (31.1)	61.5 (61.3)	74.7 (74.5)
(0.25,1.25)	42.1 (41.9)	166.6 (166.4)	164.6 (164.4)	132.4 (132.2)	36.9 (36.7)	70.3 (70.1)	142.5 (142.3)	93.1 (92.9)	54.4 (54.2)	8.5 (8.3)
(0.75,1.25)	6.3 (6.1)	64.4 (64.2)	95.2 (95.0)	124.7 (124.5)	168.5 (168.3)	14.3 (14.1)	96.9 (96.7)	133.7 (133.5)	156.1 (155.9)	124.5 (124.3)
(1.25,1.25)	2.4 (2.2)	35.1 (34.9)	55.0 (54.8)	73.5 (73.3)	129.1 (128.9)	5.2 (5.0)	57.8 (57.6)	86.0 (85.8)	109.5 (109.3)	157.9 (157.7)
(2.00,1.25)	1.4 (1.3)	17.6 (17.4)	30.3 (30.1)	42.8 (42.6)	81.1 (80.9)	2.4 (2.2)	32.1 (31.9)	49.2 (49.0)	69.4 (69.2)	120.3 (120.1)
(0.25,2.00)	6.0 (5.8)	23.4 (23.2)	31.3 (31.1)	39.3 (39.1)	57.6 (57.4)	17.9 (17.7)	49.5 (49.3)	57.7 (57.5)	63.4 (63.2)	50.3 (50.1)
(0.75,2.00)	2.9 (2.8)	13.0 (12.8)	17.6 (17.4)	22.5 (22.3)	35.3 (35.1)	9.4 (9.2)	31.0 (30.8)	39.7 (39.5)	47.5 (47.3)	59.3 (59.1)
(1.25,2.00)	2.3 (2.2)	9.6 (9.4)	13.3 (13.1)	17.2 (17.0)	27.8 (27.6)	6.8 (6.6)	24.4 (24.2)	31.9 (31.7)	37.9 (37.7)	52.5 (52.3)
(2.00,2.00)	1.5 (1.4)	4.7 (4.5)	7.0 (6.8)	9.0 (8.8)	14.9 (14.7)	1.8 (1.7)	7.3 (7.1)	10.4 (10.2)	13.3 (13.1)	21.8 (21.6)

$\theta_0 = (\gamma_0, \eta_0, \mu_0)$. To calculate the ARL_1 values, the vector of OC parameters is also defined as $\theta_1 = (\gamma_1, \eta_1, \mu_1) = (\delta_\gamma \gamma_0, \delta_\eta \eta_0, \delta_\mu \mu_0)$ where $\delta > 0$ quantifies the shift magnitude in each parameter. We set $\delta_k = 0.25, 0.75, 1.25, 2.00$ for $k = \gamma, \eta$ and μ to account for both upward and downward shifts in the associated parameters.

The results of the ARL and SDRL analysis are presented in Tables 1–5. Specifically, Tables 1–3 correspond to the power law intensity function, while Tables 3–5 pertain to the log-linear intensity function. By examining these results, we gain valuable insights into the performance and effectiveness of the proposed control charts across various scenarios and deviations from the IC condition. ARL and SDRL values in these tables are computed through Monte Carlo simulations described in Algorithm 1. Though ARL_0 can be calculated theoretically by $\mathrm{ARL}_0 = \frac{1}{\alpha}$ from (22), it could also be calculated from Algorithm 1 by generating X_i and Y_i from θ_0. Moreover, ARL_1 and SDRL_1 can be computed from Algorithm 1 by generating X_i and Y_i using θ_1.

6.1 | Sensitivity Analysis

The primary result shown by the tables is that the proposed chart is ARL-unbiased across all shift combinations and both intensity models, i.e., we always have $\mathrm{ARL}_0 > \mathrm{ARL}_1$. Now, let us continue by assessing the ability of the proposed chart to detect shifts in γ. The tables show that when $\delta_\eta < 1$, the chart usually detects downward shifts in γ sooner than its upward shifts. For example, in the power law intensity function, when $\beta = -2.00, \tau = 0.3, \delta_\eta = 0.75$ and $\delta_\mu = 0.25$, the ARL_1 (SDRL_1) corresponding to $\delta_\gamma = 0.25, 0.75, 1.25, 2.00$ are 19.7 (18.3), 55.7 (55.3), 88.6 (87.7) and 128.3 (126.5) (Table 1), respectively. On the contrary, when $\delta_\eta > 1$, the control chart detects upward shifts in γ sooner than its downward shifts. For example, in the log-linear intensity function, when $\beta = 0.00, \tau = 0.8, \delta_\eta = 2.00$ and $\delta_\mu = 2.00$, the ARL_1 (SDRL_1) corresponding to $\delta_\gamma = 0.25, 0.75, 1.25, 2.00$ are 51.9 (48.2), 41.0 (37.8), 31.5 (28.9) and 20.5 (18.8) (Table 3), respectively.

Assessing the chart's performance in detecting shifts in η is another important case due to its impact on system deterioration. An increase in the shape parameter η leads to an increase in the frequency of failures. The observed trend in the chart's ability to identify shifts in η appears consistent with its performance in detecting shifts in γ. This suggests that the chart usually detects downward (upward) shifts in η and μ sooner than their upward (downward) deviations when $\delta_\gamma < 1$ ($\delta_\gamma > 1$). For example, in the power law intensity function, when $\beta = 2.00, \tau = 0.3, \delta_\gamma = 0.25$ and $\delta_\mu = 1$, the ARL_1 (SDRL_1) corresponding to $\delta_\eta = 0.25, 0.75, 1.25, 2.00$ are 3.9 (1.2), 33.0 (32.1), 158.6 (156.7) and 112.4 (111.1) (Table 2), respectively. These findings suggest that the chart is more effective at detecting shifts in γ and η when they occur in the same direction, compared to shifts in opposite directions.

We are also interested in evaluating the performance of the chart when a shift has occurred in the mean of TC μ. As an example regarding shifts in μ, in the case of the power law intensity function when $\beta = 0.00, \tau = 0.3, \delta_\gamma = 1.25$, and $\delta_\eta = 2.00$, the ARL_1 (SDRL_1) corresponding to $\delta_\mu = 0.25, 0.75, 1.00, 1.25, 2.00$ are 13.5 (12.9), 26.9 (26.1), 33.2 (32.5), 38.9 (37.8), and 52.2 (50.6)

TABLE 3 | The ARL (SDRL) values based on power law(left) and log linear(right) intensity for $\beta = 0.00$ with $\gamma_0 = 0.05$, $\eta_0 = 1.50$, $\mu_0 = 1.00$ when $\tau = 0.3$ (upper block) and $\tau = 0.8$ (lower block).

$(\delta_\gamma, \delta_\eta)$ δ_μ	$\beta = 0.00$					$\beta = 0.00$				
	0.25	0.75	1.00	1.25	2.00	0.25	0.75	1.00	1.25	2.00
(0.25,0.25)	12.4(0.4)	2.1(0.4)	2.1(0.4)	2.0(0.3)	1.9(0.3)	11.3(10.2)	8.2(7.5)	7.7(7.0)	7.1(6.4)	6.2(5.6)
(0.75,0.25)	3.9(0.6)	3.5(0.6)	3.4(0.5)	3.3(0.5)	3.1(0.5)	17.7(16.3)	12.9(11.9)	11.8(10.8)	11.1(10.2)	9.3(8.6)
(1.00,1.00)	81.9(80.4)	182.2(181.3)	196.7(195.2)	192.5(189.8)	144.0(142.6)	79.1(73.3)	186.6(172.4)	196.9(181.5)	183.4(169.7)	142.2(132.5)
(1.25,0.25)	4.8(3.5)	4.5(3.3)	4.3(3.7)	4.2(3.6)	4.1(3.8)	27.3(24.9)	20.4(18.7)	18.7(17.2)	17.3(15.8)	14.6(13.3)
(2.00,0.25)	5.0(4.8)	5.5(5.1)	5.3(4.9)	5.2(4.8)	5.0(3.9)	48.9(45.0)	40.2(37.4)	37.1(34.5)	34.2(31.6)	29.7(27.4)
(0.25,0.75)	50.7(49.2)	22.8(21.7)	17.9(17.1)	15.2(14.9)	11.0(10.0)	126.8(117.0)	58.8(54.1)	49.5(45.5)	41.4(38.1)	28.8(26.3)
(0.75,0.75)	132.7(131.5)	64.6(63.7)	53.3(52.7)	45.5(44.7)	32.0(30.3)	165.0(152.2)	94.4(86.3)	76.6(69.8)	66.3(60.5)	45.8(42.1)
(1.25,0.75)	161.0(160.0)	106.0(104.4)	85.9(84.5)	76.8(75.6)	53.3(52.5)	151.9(141.3)	140.0(129.9)	119.1(111.2)	104.6(97.2)	74.4(69.1)
(2.00,0.75)	128.9(127.6)	150.7(149.6)	125.1(123.7)	113.5(112.9)	83.4(82.6)	62.4(57.1)	162.8(151.4)	174.9(163.5)	171.6(159.2)	141.7(131.6)
(0.25,1.25)	91.6(89.9)	177.8(177.1)	185.5(184.1)	181.0(180.3)	148.0(147.4)	71.3(66.1)	152.7(140.3)	176.3(162.0)	180.9(168.5)	163.3(151.2)
(0.75,1.25)	45.1(44.1)	105.3(104.6)	129.1(127.6)	146.8(145.4)	172.6(172.1)	50.9(47.2)	117.9(108.9)	143.0(132.6)	161.4(149.9)	177.6(164.3)
(1.25,1.25)	30.8(30.4)	76.0(74.7)	97.2(95.7)	115.0(113.4)	157.4(156.5)	35.6(32.9)	87.9(80.4)	113.6(104.8)	128.9(117.3)	169.9(156.4)
(2.00,1.25)	21.7(21.0)	58.1(57.2)	72.5(70.9)	89.7(88.0)	122.4(121.5)	20.2(18.6)	53.9(49.6)	67.5(62.0)	84.5(77.3)	119.0(109.8)
(0.25,2.00)	22.5(21.8)	47.2(46.1)	57.8(56.7)	65.6(64.4)	89.3(87.7)	24.3(22.1)	52.5(48.3)	62.6(58.0)	71.8(66.5)	94.6(87.2)
(0.75,2.00)	15.6(15.0)	31.8(30.6)	38.8(37.4)	45.1(43.5)	61.7(60.0)	20.9(19.1)	43.6(40.2)	53.0(49.3)	60.0(56.0)	82.5(76.9)
(1.25,2.00)	13.5(12.9)	26.9(26.1)	33.2(32.5)	38.9(37.8)	52.2(50.6)	16.6(15.2)	36.4(33.8)	44.3(41.2)	51.6(48.3)	68.3(63.4)
(2.00,2.00)	11.2(10.7)	23.7(22.9)	28.0(27.1)	33.6(32.4)	46.0(44.9)	12.3(11.2)	27.5(25.3)	32.8(30.2)	39.3(36.0)	54.1(50.2)
(0.25,0.25)	1.7(1.6)	1.5(1.4)	1.4(1.3)	1.4(1.3)	1.3(1.2)	5.7(5.1)	3.9(3.4)	3.5(3.1)	3.2(2.9)	2.6(2.3)
(0.75,0.25)	1.7(1.6)	1.9(1.8)	1.9(1.8)	1.9(1.8)	1.9(1.8)	9.0(8.3)	6.1(5.5)	5.5(4.9)	4.8(4.3)	3.9(3.4
(1.00,1.00)	6.0(5.8)	163.7(162.3)	197.6(196.2)	180.7(179.3)	90.7(89.8)	)17.4(15.9)	155.9(144.2)	196.6(183.4)	171.7(159.3)	90.9(84.1)
(1.25,0.25)	1.3(1.2)	1.8(1.7)	1.7(1.6)	1.9(1.8)	2.0(1.9))	13.7(12.4)	10.4(9.6)	9.2(8.4)	8.2(7.5)	6.4(5.8)
(2.00,0.25)	1.0(0.9)	1.4(1.3)	1.4(1.3)	1.6(1.5)	1.8(1.7)	2.9(2.6)	22.9(20.7)	21.4(19.4)	19.8(17.9)	16.1(14.6)
(0.25,0.75)	15.3(15.1)	4.0(3.9)	3.2(3.1)	2.7(2.6)	2.2(2.1)	80.2(73.4)	20.3(18.4)	14.2(13.0)	10.2(9.3)	5.4(4.8)
(0.75,0.75)	29.3(29.1)	24.7(24.5)	17.3(17.1)	13.1(12.9)	6.9(6.8)	131.8(122.3)	48.0(43.7)	33.1(30.1)	24.2(22.1)	12.8(11.6)
(1.25,0.75)	9.7(9.5)	55.3(55.1)	41.3(41.1)	30.9(30.7)	17.1(16.9)	65.4(59.9)	100.0(91.7)	74.9(68.8)	55.8(51.1)	30.8(28.3)

(Continues)

TABLE 3 | (Continued)

$(\delta_\gamma, \delta_\eta)\, \delta_\mu$	$\beta = 0.00$					$\beta = 0.00$				
	0.25	0.75	1.00	1.25	2.00	0.25	0.75	1.00	1.25	2.00
(2.00,0.75)	1.2 (1.1)	65.3 (65.1)	76.4 (76.2)	63.0 (62.8)	36.8 (36.6)	1.3 (1.2)	112.5 (103.3)	147.4 (136.9)	144.1 (134.0)	101.3 (94.2)
(0.25,1.25)	32.8 (32.6)	147.3 (147.1)	162.7 (162.5)	157.5 (157.3)	60.3 (60.1)	22.8 (20.9)	115.1 (106.5)	149.9 (139.3)	165.1 (153.4)	114.7 (106.1)
(0.75,1.25)	4.5 (4.3)	52.1 (51.9)	80.4 (80.2)	103.9 (103.7)	153.2 (153.0)	10.7 (9.7)	68.8 (62.5)	100.6 (92.1)	128.4 (118.9)	160.1 (148.7)
(1.25,1.25)	1.8 (1.6)	27.3 (27.1)	43.3 (43.1)	60.9 (60.7)	110.9 (110.7)	3.5 (3.2)	37.4 (34.1)	57.3 (52.6)	80.2 (73.9)	134.3 (125.1)
(2.00,1.25)	1.3 (1.2)	12.7 (12.5)	23.4 (23.2)	34.5 (34.3)	69.3 (69.1)	1.2 (1.1)	12.3 (11.1)	21.5 (19.7)	31.5 (28.4)	65.4 (60.2)
(0.25,2.00)	3.8 (3.6)	16.3 (16.1)	21.9 (21.7)	27.6 (27.4)	42.2 (42.0)	5.1 (4.7)	19.2 (17.3)	26.0 (23.6)	32.9 (30.0)	51.9 (48.2)
(0.75,2.00)	2.1 (2.0)	8.7 (8.5)	12.0 (11.8)	15.6 (15.4)	25.1 (24.9)	3.4 (3.1)	14.2 (12.9)	20.0 (18.2)	25.7 (23.6)	41.0 (37.8)
(1.25,2.00)	1.7 (1.6)	6.2 (6.0)	9.0 (8.8)	11.9 (11.7)	19.1 (18.9)	2.1 (1.9)	10.1 (9.2)	14.6 (13.4)	18.7 (17.0)	31.5 (28.9)
(2.00,2.00)	1.5 (1.4)	4.7 (4.5)	7.0 (6.8)	9.0 (8.8)	14.9 (14.7)	1.2 (1.1)	5.3 (4.8)	8.4 (7.6)	11.2 (10.1)	20.5 (18.8)

(Table 3), respectively. Similarly, for the log-linear intensity function under the same configuration of $\beta = 2.00$, $\tau = 0.8$, $\delta_\gamma = 1.25$, and $\delta_\eta = 2.00$, the ARL_1 (SDRL_1) values corresponding to $\delta_\mu = 0.25, 0.75, 1.00, 1.25, 2.00$ are 34.8 (32.1), 48.4 (44.1), 62.4 (57.2), and 98.3 (89.5) (Table 5), respectively.

It is well known that the risk factors impact the failure mechanism of the system. On the other hand, we know that $\beta = 0$ suggests no effect of the risk factor on the hazard rate. In this case, the chart's sensitivity to shifts remains at a baseline level, not influenced by the risk factor. By looking at the tables, it can be observed that the control chart declares an OC alarm when $\beta < 0\,(\beta > 0)$ sooner (later) than in the scenario of the absence of a risk factor, denoted by $\beta = 0$. For example, in the log-linear intensity function, when $\tau = 0.3$, $\delta_\gamma = 0.25$, $\delta_\eta = 2.00$ and $\delta_\mu = 1.00$, the ARL_1 corresponding to $\beta = -2.00, -0.50, 0.50, 2.00$ are 36.9 and 48.1 (from Table 4) and 78.4 and 128.9 (from Table 5), respectively. This indicates that risk factors exhibiting a negative association with TBE have a positive impact on the performance of the proposed chart, while those with a positive association negatively impact the efficiency of the monitoring technique. This insight stands out as a key finding in our simulation study. This trend could be justified by understanding how the sign of β relates to the sensitivity of the control chart to detect shifts. A $\beta < 0$ suggests a reduction in the hazard rate associated with the risk factor, implying that the effect of the risk factor is associated with a lower likelihood of the shift occurring. Consequently, the chart is more sensitive to changes, detecting shifts sooner because the risk factor is acting as a mitigating or stabilizing factor. On the other hand, a $\beta > 0$ implies an increase in the hazard rate associated with the risk factor, suggesting that the risk factor is associated with an elevated likelihood of the shift occurring. Thus, the chart is less sensitive to changes, detecting shifts later, as the risk factor contributes to a higher baseline risk of shifts.

It can also be observed from the tables that the dependency parameter τ noticeably affects the OC performance of the proposed monitoring scheme. From the tables, ARL_1 decreases when τ increases. This means that the chart detects the OC conditions sooner when the degree of dependency between TBE and TC is stronger. Thus, the higher degree of dependency between TBE and TC improves the performance of the chart. This finding is also a crucial outcome of our simulation study. This could be justified by the fact that when there is a higher degree of dependency between TBE and TC, it implies that they are more closely related or influenced by each other. As a result, changes in one variable are likely to be reflected in the other and consequently, the chart becomes more sensitive to changes in the joint distribution of the two variables.

6.2 | Performance Comparison

The study conducted by Ali [50] introduced a control chart for monitoring the TBE based on the NHPP with power law intensity, without accounting for risk factors and the TC variable. In this subsection, we evaluate the performance of the proposed chart in comparison to Ali's chart, using the ARL metric. In the initial phase, we generate 5000 TBEs with parameters $\gamma_0 = 0.05$, $\eta_0 = 1.50$, and $\beta = 0.50, 2.00$ using the RANHPP (risk-adjusted NHPP) model. Then the parameters are estimated using the

TABLE 4 | The ARL (SDRL) values based on log-linear intensity for $\beta = -2.00, -0.50$ with $\gamma_0 = 0.05$, $\eta_0 = 2.00$, $\mu_0 = 1.00$ when $\tau = 0.3$ (upper block) and $\tau = 0.8$ (lower block).

$(\delta_\gamma, \delta_\eta)\ \delta_\mu$	$\beta = -2.00$					$\beta = -0.50$				
	0.25	0.75	1.00	1.25	2.00	0.25	0.75	1.00	1.25	2.00
(0.25,0.25)	3.4 (3.1)	3.3 (3.0)	3.2 (2.9)	3.1 (2.8)	2.5 (2.3)	7.1 (6.8)	5.5 (5.2)	5.2 (4.9)	4.9 (4.6)	4.4 (4.1)
(0.75,0.25)	3.8 (3.5)	3.9 (3.6)	3.8 (3.5)	3.8 (3.5)	2.9 (2.7)	10.6 (9.1)	8.1 (7.8)	7.4 (7.1)	7.0 (6.7)	6.1 (5.8)
(1.00,1.00)	56.9 (53.0)	162.5 (159.1)	199.0 (196.7)	206.5 (203.6)	132.6 (129.1)	81.4 (78.0)	179.2 (176.6)	198.1 (195.1)	184.2 (181.7)	144.1 (141.7)
(1.25,0.25)	4.3 (4.0)	4.7 (4.4)	4.6 (4.3)	4.5 (4.2)	3.4 (3.1)	16.3 (15.0)	12.4 (11.1)	11.3 (10.0)	10.6 (9.3)	9.3 (8.0)
(2.00,0.25)	5.2 (4.9)	5.9 (5.6)	5.9 (5.6)	5.7 (5.4)	4.6 (4.3)	31.1 (29.1)	24.5 (22.5)	22.3 (20.3)	20.9 (18.9)	17.8 (15.8)
(0.25,0.75)	30.9 (27.9)	23.6 (20.6)	19.8 (16.8)	19.0 (16.0)	11.2 (8.3)	105.7 (102.7)	50.2 (47.2)	39.7 (36.3)	33.6 (30.6)	23.6 (20.6)
(0.75,0.75)	53.3 (50.3)	49.1 (46.1)	43.3 (40.3)	36.7 (33.7)	17.0 (14.7)	150.9 (147.9)	80.0 (77.0)	64.8 (61.8)	54.0 (51.9)	37.7 (34.4)
(1.25,0.75)	64.1 (61.1)	97.3 (94.3)	86.8 (83.8)	76.7 (73.3)	27.3 (24.3)	169.1 (166.1)	122.8 (119.8)	99.7 (96.7)	89.6 (86.6)	62.3 (59.3)
(2.00,0.75)	36.5 (33.1)	127.9 (124.9)	144.4 (141.4)	147.9 (144.7)	54.0 (51.0)	84.4 (81.4)	169.8 (166.8)	167.4 (164.3)	151.2 (148.2)	119.9 (116.9)
(0.25,1.25)	44.9 (41.9)	129.3 (126.6)	166.6 (163.6)	188.9 (185.3)	148.4 (145.3)	60.8 (57.8)	140.3 (137.3)	162.2 (159.3)	178.1 (175.1)	176.3 (173.3)
(0.75,1.25)	31.4 (28.4)	106.8 (103.2)	140.7 (137.7)	169.4 (166.4)	122.2 (119.8)	45.0 (42.0)	104.0 (101.0)	130.4 (127.4)	148.9 (145.9)	176.1 (173.1)
(1.25,1.25)	21.9 (18.5)	75.5 (72.5)	98.9 (95.9)	122.7 (119.7)	93.0 (90.7)	30.8 (27.8)	74.7 (71.7)	98.7 (95.7)	113.8 (110.4)	152.5 (149.5)
(2.00,1.25)	11.9 (10.4)	44.9 (42.4)	59.3 (56.3)	76.3 (73.3)	58.3 (55.4)	18.1 (15.1)	46.8 (43.8)	61.5 (58.5)	70.9 (67.8)	104.6 (101.6)
(0.25,2.00)	11.0 (9.7)	28.2 (25.9)	36.9 (34.6)	45.2 (42.9)	25.2 (22.9)	18.6 (16.3)	39.2 (36.9)	48.1 (45.8)	53.4 (51.1)	74.0 (71.7)
(0.75,2.00)	8.8 (7.6)	23.2 (21.0)	29.5 (27.3)	37.0 (34.8)	21.6 (19.4)	15.8 (13.6)	33.0 (30.8)	40.2 (38.0)	47.1 (44.9)	65.0 (62.8)
(1.25,2.00)	7.4 (6.1)	18.7 (16.4)	24.5 (22.2)	13.8 (11.5)	18.6 (16.3)	13.0 (10.7)	28.1 (25.8)	33.7 (31.4)	39.7 (37.4)	53.0 (50.7)
(2.00,2.00)	5.8 (4.5)	15.4 (13.1)	19.0 (16.7)	10.8 (8.5)	14.6 (12.3)	9.8 (7.5)	21.0 (18.7)	25.7 (23.4)	30.7 (28.4)	42.3 (40.0)
(0.25,0.25)	2.4 (2.1)	2.3 (2.0)	2.2 (2.0)	2.2 (2.1)	2.1 (1.9)	3.9 (3.6)	3.0 (2.7)	2.8 (2.5)	2.6 (2.4)	2.3 (2.1)
(0.75,0.25)	2.7 (2.5)	2.4 (2.2)	2.4 (2.3)	2.3 (2.1)	2.3 (2.1)	5.6 (5.2)	4.1 (3.7)	3.7 (3.3)	3.5 (3.2)	3.0 (2.7)
(1.00,1.00)	7.1 (6.6)	157.6 (144.1)	198.4 (190.3)	177.2 (163.7)	92.4 (87.9)	13.4 (12.6)	161.9 (151.2)	198.5 (186.8)	166.0 (155.9)	87.5 (83.1)
(1.25,0.25)	3.0 (2.7)	2.8 (2.6)	2.7 (2.5)	2.7 (2.4)	2.5 (2.3)	7.6 (6.9)	6.2 (5.7)	5.7 (5.2)	5.1 (4.8)	4.3 (3.9)
(2.00,0.25)	2.4 (2.2)	3.6 (3.2)	3.6 (3.3)	3.4 (3.0)	3.2 (2.9)	2.7 (2.5)	13.0 (12.1)	12.0 (11.0)	11.1 (10.3)	9.1 (8.4)
(0.25,0.75)	13.6 (12.2)	5.4 (5.0)	4.4 (4.0)	3.8 (3.5)	2.9 (2.6)	56.9 (51.3)	14.8 (13.5)	10.3 (9.7)	7.6 (6.8)	4.4 (4.0)
(0.75,0.75)	25.4 (23.1)	10.1 (9.1)	7.5 (6.9)	6.2 (5.6)	4.2 (3.9)	98.4 (92.1)	34.7 (31.8)	23.4 (21.6)	17.7 (16.3)	9.3 (8.6)
(1.25,0.75)	36.6 (33.3)	22.1 (20.5)	15.7 (14.3)	12.2 (11.1)	7.4 (6.9)	69.2 (63.7)	75.7 (70.4)	55.3 (51.6)	40.8 (37.5)	22.6 (20.8)

TABLE 4 | (Continued)

$(\delta_\gamma, \delta_\eta), \delta_\mu$	$\beta = -2.00$					$\beta = -0.50$				
	0.25	0.75	1.00	1.25	2.00	0.25	0.75	1.00	1.25	2.00
(2.00,0.75)	17.3(15.8)	67.6(61.9)	51.6(48.2)	39.5(36.1)	22.5(20.3)	1.3(1.2)	130.4(122.6)	135.3(127.9)	119.2(111.6)	76.2(70.4)
(0.25,1.25)	3.8(3.5)	38.6(35.1)	61.3(56.2)	78.4(71.6)	132.7(122.1)	16.5(15.0)	94.8(88.2)	129.4(121.1)	149.6(138.5)	142.9(132.3)
(0.75,1.25)	2.3(2.1)	20.3(18.6)	33.5(30.7)	46.3(42.8)	86.3(80.1)	6.5(5.9)	54.7(50.3)	81.8(75.2)	107.6(98.4)	163.5(152.1)
(1.25,1.25)	1.6(1.5)	10.3(9.4)	17.5(16.1)	25.8(23.5)	52.0(47.7)	2.4(2.2)	29.2(27.1)	46.2(42.7)	65.8(60.1)	113.4(105.2)
(2.00,1.25)	1.3(1.2)	3.9(3.5)	6.6(6.1)	10.2(9.3)	21.8(20.0)	1.2(1.1)	9.1(8.3)	16.2(14.9)	24.6(22.3)	52.7(48.9)
(0.25,2.00)	1.6(1.5)	3.7(3.4)	4.5(4.1)	5.4(4.9)	7.9(7.1)	3.1(2.8)	12.3(11.2)	16.9(15.2)	21.5(19.6)	34.7(32.0)
(0.75,2.00)	1.5(1.4)	3.1(2.9)	3.9(3.5)	4.6(4.3)	6.7(6.1)	2.2(2.0)	9.1(8.3)	12.9(11.6)	16.4(15.1)	27.1(24.9)
(1.25,2.00)	1.3(1.2)	2.7(2.5)	3.4(3.1)	4.0(3.6)	5.6(5.1)	1.6(1.4)	6.6(6.1)	9.4(8.6)	12.4(11.4)	21.1(19.0)
(2.00,2.00)	1.2(1.1)	2.1(1.9)	2.6(2.4)	3.1(2.8)	4.4(4.1)	1.1(1.0)	3.5(3.2)	5.4(5.0)	7.3(6.7)	13.3(12.0)

IFM approach explained in the Appendix. For the proposed model with $\beta = 0.50$, the estimated parameters are $\hat{\gamma} = 0.05$, $\hat{\eta} = 1.52$, and $\hat{\beta} = 0.52$ that are fairly close the known values. In contrast, the NHPP-based method proposed by [50] yields parameter estimates of $\hat{\gamma} = 0.11$ and $\hat{\eta} = 1.43$. These biased estimates, especially in the case of γ, are caused by the noise incurred by the risk factor that has not been accounted for in the estimation process. This unaccounted noise is expected to impact the chart's performance.

Given the estimated parameters, we calculated the control limits of the proposed method (by ignoring TC) from the conditional CDF of X_i given in (14) and the limits of the alternative method from [50]. This means that the risk factor is ignored in the design of the alternative approach. Then, the performance of both approaches is compared using the ARL metric across 17 combinations of $(\delta_\gamma, \delta_\eta)$. Table 6 presents the ARL values of the RANHPP-based and NHPP-based methods when monitoring TBEs in the presence of a risk factor. The crucial finding in the table is that, while Ali's approach detects some shifts sooner than the proposed method, its actual ARL_0 consistently falls below the target value of 200. Specifically, the IC ARL for this approach is 187.56 and 28.65 when $\beta = 0.50$ and $\beta = 2.00$, respectively. Ultimately, it can be concluded that although the alternative approach outperforms in some instances, this improved performance comes at the cost of generating numerous false alarms, particularly when β is relatively large. These frequent alarms lose their warning role and are unlikely to trigger an audit each time.

6.3 | The Impact of Ignoring the Risk Factor

We further investigate the impact of the risk factors on the IC performance of the proposed chart that has been designed with ignorance of the risk factor. In other words, we are interested in understanding the consequences of a risk factor affecting TBE that has not been considered in the design of the corresponding chart. To do this, we follow the Algorithm 1 except for steps 10 and 11 where we calculate the control limits from the CDF of W_i in (20) that is not conditioned on $\boldsymbol{z}_i$. The simulation setting is based on the parameters mentioned earlier in this section with a nominal $ARL_0 = 200$. The results of this study (not presented here) showed that the actual false alarm rate of the chart is considerably higher than its nominal value. This observation aligns with our findings when comparing the results with those of [50]. For example, the ARL_0 values corresponding to $\beta = -2.00, -0.50, 0.50, 2.00$ were $6.83, 111.72, 96.37$, and 4.33, respectively. These findings highlight the noticeable influence of neglecting the risk factors on the statistical properties of the monitoring technique.

7 | A Case Study: Monitoring Pipeline Accidents

In this section, our objective is to apply the suggested control chart within an SPM context for the analysis of pipeline accident data briefly introduced in Section 2. The dataset in question contains an extensive set of oil pipeline accidents, including leaks and spills. Our primary goal is to explore how the proposed

TABLE 5 | The ARL (SDRL) values based on log-linear intensity for $\beta = 0.50, 2.00$ with $\gamma_0 = 0.05, \eta_0 = 2.00, \mu_0 = 1.00$ when $\tau = 0.3$ (upper block) and $\tau = 0.8$ (lower block).

$(\delta_\gamma, \delta_\eta)\ \delta_\mu$	$\beta = 0.50$					$\beta = 2.00$				
	0.25	0.75	1.00	1.25	2.00	0.25	0.75	1.00	1.25	2.00
(0.25,0.25)	17.4(15.8)	12.6(11.7)	11.3(10.4)	10.6(9.8)	9.0(8.3)	51.7(47.5)	34.7(31.9)	30.2(27.5)	26.8(24.6)	22.0(20.3)
(0.75,0.25)	27.9(25.4)	19.8(18.0)	17.8(16.3)	16.9(15.1)	14.0(12.9)	77.0(70.8)	54.2(49.7)	47.8(44.1)	43.7(40.5)	35.6(32.3)
(1.00,1.00)	80.9(75.2)	176.2(165.3)	195.8(182.6)	182.1(169.9)	146.0(135.8)	84.3(78.9)	180.3(168.5)	199.0(184.2)	194.2(181.0)	150.8(140.6)
(1.25,0.25)	42.4(39.1)	31.4(28.9)	28.6(26.7)	26.7(24.8)	22.3(20.5)	102.2(95.8)	86.4(79.6)	76.5(70.7)	72.1(67.4)	57.2(53.1)
(2.00,0.25)	67.0(61.4)	60.3(56.2)	56.5(52.9)	52.8(48.7)	45.8(42.0)	64.3(60.1)	128.9(120.4)	129.3(121.6)	124.8(115.9)	111.2(102.4)
(0.25,0.75)	146.4(135.2)	72.7(67.4)	56.0(51.8)	48.6(44.5)	35.4(32.3)	171.1(159.8)	104.7(98.5)	84.8(78.6)	70.3(65.1)	49.1(45.3)
(0.75,0.75)	175.4(161.2)	112.2(104.7)	94.3(87.9)	77.3(71.5)	54.9(50.8)	165.0(154.1)	156.9(146.4)	130.1(121.7)	113.9(106.2)	79.3(74.1)
(1.25,0.75)	146.3(134.7)	164.7(154.9)	136.3(126.5)	121.9(113.4)	90.7(84.3)	96.9(89.2)	183.3(172.5)	178.2(165.8)	164.8(153.7)	124.8(115.9)
(2.00,0.75)	49.6(45.7)	163.0(151.6)	173.3(160.9)	178.5(165.2)	156.6(144.2)	34.4(31.9)	114.8(107.5)	153.8(143.5)	171.0(159.3)	181.6(169.1)
(0.25,1.25)	79.7(73.8)	165.0(153.4)	181.8(170.0)	179.4(167.8)	160.3(149.2)	104.1(97.2)	186.6(174.5)	183.0(172.1)	171.4(160.2)	121.8(113.7)
(0.75,1.25)	58.7(53.6)	137.2(127.8)	158.1(146.3)	173.0(159.5)	176.4(163.1)	72.9(67.2)	160.5(148.3)	177.2(163.9)	180.4(166.5)	167.9(155.1)
(1.25,1.25)	40.3(36.7)	103.6(95.7)	131.0(121.2)	142.5(132.0)	177.3(164.5)	52.2(48.1)	129.3(120.1)	148.3(137.2)	165.4(152.0)	189.1(174.2)
(2.00,1.25)	23.3(21.1)	61.3(56.2)	78.5(72.3)	92.7(85.5)	131.5(122.3)	27.2(25.0)	74.4(69.3)	99.1(91.2)	113.8(105.2)	152.5(141.6)
(0.25,2.00)	31.0(28.9)	65.9(60.8)	78.4(72.3)	88.6(82.4)	117.1(108.2)	53.3(48.9)	113.2(105.6)	128.9(119.2)	142.5(132.1)	157.8(146.2)
(0.75,2.00)	25.8(23.4)	54.3(49.7)	66.0(60.4)	77.1(70.8)	103.3(94.6)	44.0(40.1)	94.2(87.5)	113.3(105.1)	126.4(117.6)	154.0(143.7)
(1.25,2.00)	21.3(19.4)	46.2(42.6)	57.3(52.8)	64.5(59.4)	85.7(79.1)	34.4(31.7)	77.7(71.4)	93.2(85.6)	108.5(99.7)	141.5(129.6)
(2.00,2.00)	14.8(13.3)	34.3(31.5)	42.3(39.1)	50.0(45.8)	66.6(61.1)	22.1(20.1)	54.7(50.4)	68.6(63.0)	80.3(74.2)	109.3(101.6)
(0.25,0.25)	9.0(8.1)	5.5(5.0)	4.8(4.3)	4.3(3.8)	3.2(2.9)	30.9(28.4)	16.0(14.7)	12.9(11.9)	10.5(9.6)	6.3(5.7)
(0.75,0.25)	15.1(13.9)	9.5(8.7)	8.3(7.6)	7.3(6.7)	5.5(5.0)	49.4(45.7)	32.0(29.3)	26.1(24.0)	22.0(20.1)	14.3(13.1)
(1.00,1.00)	19.8(18.1)	168.2(155.7)	198.9(185.0)	177.6(163.9)	88.4(80.3)	19.4(17.8)	166.2(153.0)	197.3(182.4)	173.0(160.6)	90.7(82.7)
(1.25,0.25)	22.3(20.6)	17.6(16.1)	14.9(13.7)	13.4(12.1)	10.0(9.1)	38.5(35.1)	58.5(53.7)	50.7(46.2)	43.4(39.8)	30.9(28.3)
(2.00,0.25)	2.0(1.8)	36.0(33.0)	35.6(32.8)	32.6(30.3)	26.5(24.3)	1.4(1.3)	71.1(66.7)	85.1(78.6)	92.6(85.3)	80.1(73.4)
(0.25,0.75)	103.4(95.2)	27.4(25.1)	18.8(17.0)	13.5(12.1)	6.7(6.1)	153.9(144.5)	53.3(48.7)	34.5(31.2)	24.2(22.0)	10.8(9.7)
(0.75,0.75)	148.0(137.6)	63.0(58.3)	43.7(40.0)	33.1(30.1)	16.9(15.1)	99.8(92.1)	113.3(104.6)	82.6(75.2)	62.5(57.0)	30.4(27.1)

(Continues)

TABLE 5 | (Continued)

$(\delta_\gamma, \delta_\eta)$, δ_μ	$\beta = 0.50$					$\beta = 2.00$				
	0.25	0.75	1.00	1.25	2.00	0.25	0.75	1.00	1.25	2.00
(1.25,0.75)	50.5(46.4)	126.4(117.3)	95.6(88.1)	76.1(70.2)	41.0(37.1)	14.6(13.3)	167.3(156.1)	148.9(138.5)	128.2(119.7)	74.5(69.0)
(2.00,0.75)	1.3(1.2)	91.3(84.7)	145.2(135.1)	147.7(137.4)	124.0(115.5)	1.4(1.3)	36.2(33.1)	83.4(76.9)	131.3(122.4)	172.2(160.6)
(0.25,1.25)	29.4(27.1)	132.9(124.0)	163.3(151.9)	169.2(158.0)	89.8(82.1)	47.2(43.8)	171.6(160.3)	163.9(152.7)	122.7(113.2)	38.7(35.1)
(0.75,1.25)	14.5(13.3)	85.2(78.3)	121.2(112.0)	148.4(138.1)	163.5(151.7)	22.1(20.3)	125.4(117.0)	161.1(149.3)	178.2(164.9)	123.1(114.3)
(1.25,1.25)	5.3(4.8)	46.7(42.5)	69.0(63.1)	96.1(88.0)	154.5(142.6)	8.4(7.7)	72.0(66.8)	108.0(99.7)	135.2(125.0)	177.4(165.3)
(2.00,1.25)	1.3(1.2)	15.6(14.1)	26.0(23.9)	39.2(35.7)	79.0(72.1)	1.4(1.3)	21.0(19.0)	37.5(34.0)	56.8(52.3)	114.6(105.7)
(0.25,2.00)	7.8(7.1)	27.8(25.5)	38.0(35.0)	47.7(43.7)	70.8(65.5)	19.8(18.3)	66.5(61.2)	83.9(78.4)	100.9(92.6)	107.8(99.3)
(0.75,2.00)	5.2(4.7)	21.4(19.8)	29.1(26.9)	37.3(34.1)	58.5(53.6)	12.3(11.2)	50.4(46.6)	67.9(62.3)	82.8(76.7)	114.3(105.4)
(1.25,2.00)	2.9(2.6)	15.5(14.2)	21.6(19.8)	27.2(25.1)	45.7(41.3)	5.9(5.3)	34.8(32.1)	48.4(44.1)	62.4(57.2)	98.3(89.5)
(2.00,2.00)	1.2(1.1)	7.7(6.9)	12.1(11.0)	16.4(15.0)	29.5(26.9)	1.3(1.2)	15.3(14.1)	23.8(21.9)	34.8(32.1)	63.1(58.0)

TABLE 6 | ARL values of the RANHPP and the NHPP TBE control charts.

$(\delta_\gamma, \delta_\eta)$	$\beta = 0.50$		$\beta = 2.00$	
	RANHPP	**NHPP**	**RANHPP**	**NHPP**
(0.25,0.25)	1.06	1.07	1.33	1.54
(0.75,0.25)	1.19	1.20	1.65	2.08
(1.00,1.00)	198.98	187.56	197.43	28.65
(1.25,0.25)	1.28	1.32	1.92	2.38
(2.00,0.25)	1.41	1.46	2.17	2.83
(0.25,0.75)	1.62	1.76	2.21	4.28
(0.75,0.75)	3.60	4.20	6.13	30.73
(1.25,0.75)	6.64	7.95	13.24	45.59
(2.00,0.75)	13.37	16.72	30.21	35.01
(0.25,1.25)	196.56	146.54	142.16	27.37
(0.75,1.25)	105.7	87.95	141.2	19.42
(1.25,1.25)	73.28	64.16	102.2	17.18
(2.00,1.25)	55.68	44.79	72.51	14.75
(0.25,2.00)	29.12	26.18	48.05	13.52
(0.75,2.00)	20.58	18.4	35.76	11.92
(1.25,2.00)	17.61	16.32	30.72	10.78
(2.00,2.00)	15.35	41.32	26.54	9.16

method can be effectively utilized and demonstrate the steps involved in its implementation using this dataset as a case study.

7.1 | Data Description

Following the details outlined in Section 2, it encompasses a collection of 2,781 records documenting oil pipeline accidents, encompassing leaks or spills, which were reported to the PHMSA during the period spanning from 2010 to 2017. While the letter-value plots in Figure 3a,b show a few outliers in TBEs and TCs, we decided to keep them and apply the proposed method. Table 9 presents the information on the last 50 accidents.

The accident date variable denotes the precise date of the oil spill, and it will serve as the basis for calculating the TBE, represented as X_i and measured in hours. The TC variable represents the sum of various costs, including Property Damage Costs, Lost Commodity Costs, Public/Private Property Damage Costs, Emergency Response Costs, Environmental Remediation Costs, and Other Costs (which be measured by 100,000 USDs), and will be denoted by Y_i. Additionally, there are five confounding variables that will be used as risk factors which are shown in Table 7.

Panels (a)–(c) of Figure 5 show the observations of the X (TBE) and Y (TC) variables along with the W's against the time index i. In this Figure, panel (a) reveals that a substantial portion of the TBE falls within the 0 to 50h range. Meanwhile, panel (b) illustrates that the TC of failures typically ranges from 0 to 5 million USD. Consequently, this suggests that the AC for most

**TABLE 7** | Information on risk factors.

| Covariate	Description
Pipeline location (PL)	Classifies pipelines into two categories: (1) onshore (ONS) or (2) offshore (OFS).
Pipeline type (PT)	Categorizes pipelines as follows: (1) Aboveground (ABG), (2) Underground (UNG), (3) Tank (TAN), or (4) Transition Area pipelines (TRA).
Liquid type (LT)	Discriminates between various liquid oil types, including (1) Biofuel/Alternative Fuel (BAF), (2) CO2, (3) Crude Oil (CRO), (4) HVL or Other Flammable or Toxic Fluid, GA (HFT), and (5) Refined and/or Petroleum Product (RPL).
Accident state (AS)	The report provides data for forty-six states across the US.
Oil Cause categories (CC)	Encompasses the following categories: (1) All other causes (AOC), (2) Other outside force damage (OFD), (3) Corrosion (COR), (4) Excavation damage (EXD), (5) Incorrect operation (INO), (6) Material/Weld/Equip failure (MWE), and (7) Natural force damage (NFD).
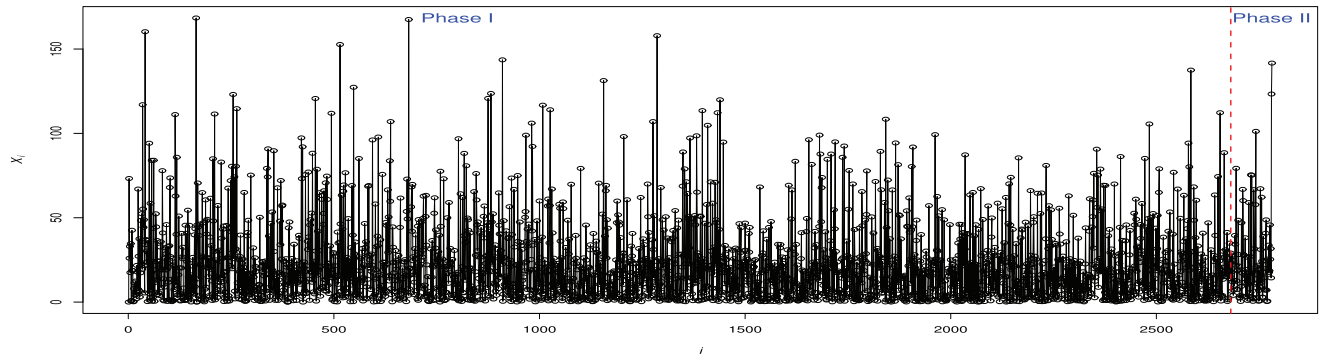
(a) TBE X_i.
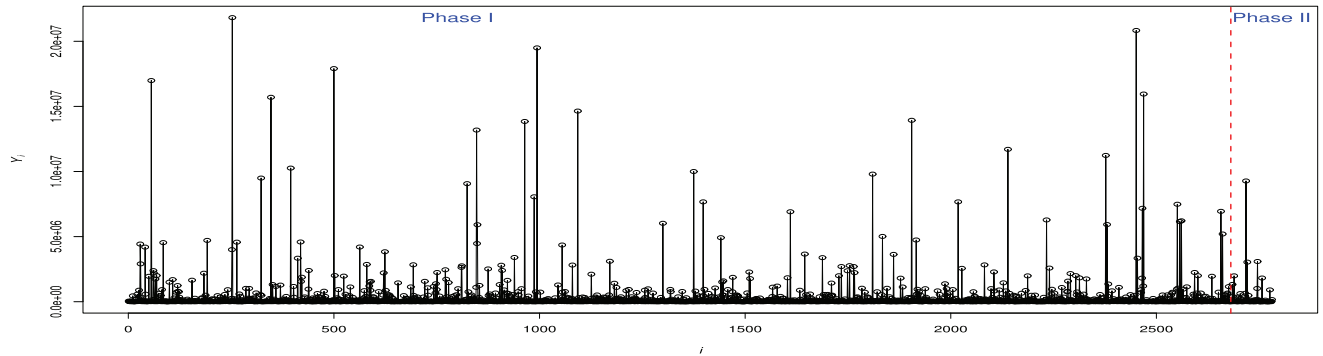
(b) TC Y_i.
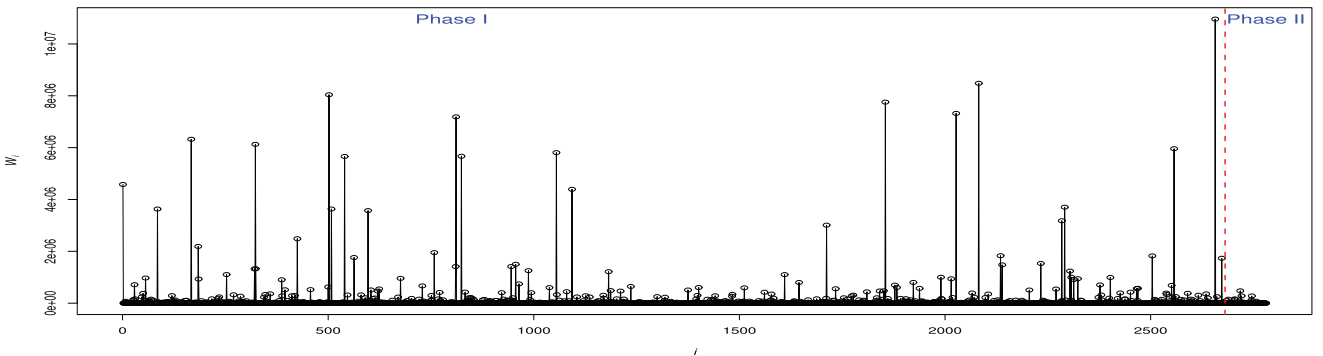
(c) AC W_i.

FIGURE 5 | Pipelines accidents raw data.

TABLE 8 | Estimated parameters of the power law RANHPP model for pipeline accidents data.
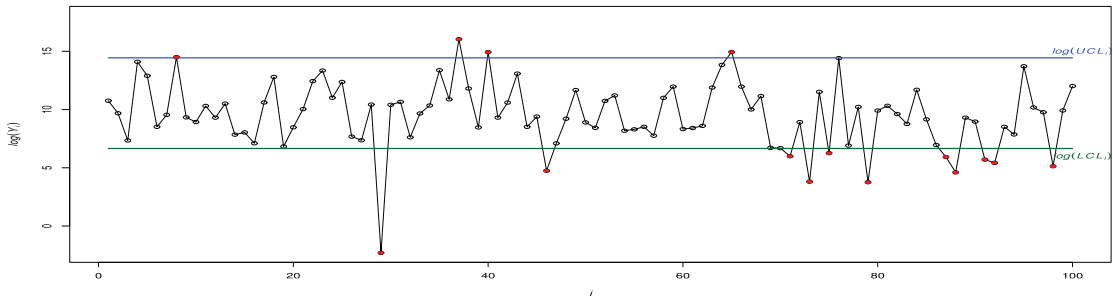
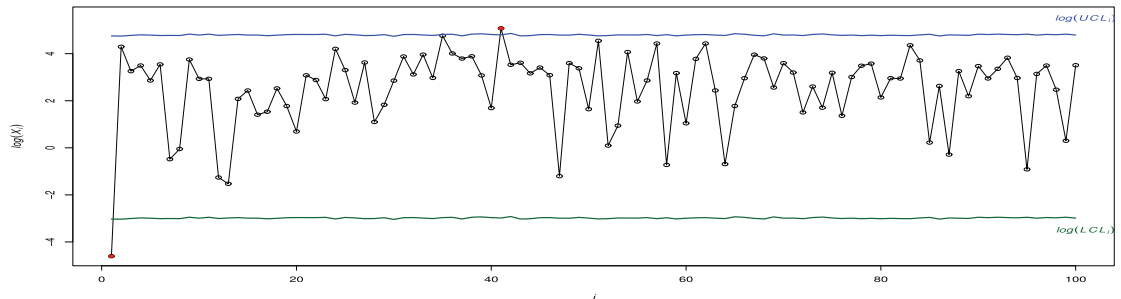|	$\hat{\gamma}$	$\hat{\eta}$	$\hat{\beta}_1$	$\hat{\beta}_2$	$\hat{\beta}_3$	$\hat{\beta}_4$	$\hat{\beta}_5$	$\hat{\mu}$	Copula	$\hat{\tau}$	AIC
	0.024	1.071	−0.131	0.002	0.016	0.001	0.010	3.21e-06	Gumbel	0.001	−95039.97
HR →	—	—	0.877	1.002	1.016	1.001	1.010	—	—		
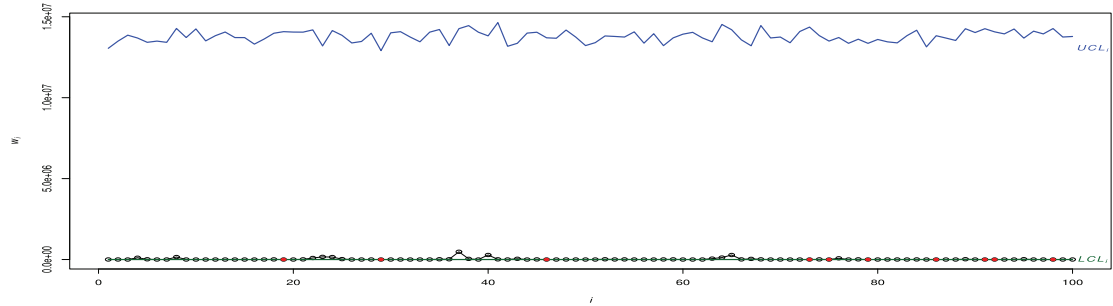
(a) Control chart based on original observations.
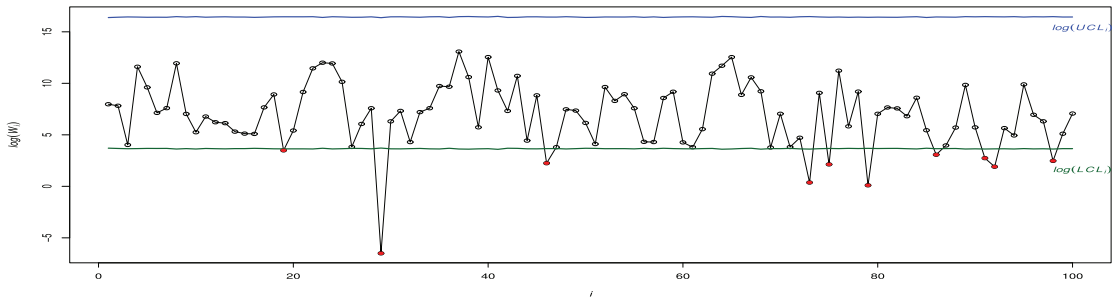
(b) Control chart for W_i based on log-transformed observations and control limits.

(c) Control chart for Y_i based on log-transformed observations and control limits.

(d) Control chart for X_i based on log-transformed observations and control limits.

FIGURE 6 | Control chart for pipeline accidents in Phase II.

failures is close to 100,000 USD, as depicted in panel (c) of Figure 5.

7.2 | Estimating the Process Parameters

For illustration purposes, we randomly selected the last 100 data points for monitoring purposes in Phase II and the rest of them are used to estimate the process parameters. To estimate the parameters, we employed the IFM approach explained in the Appendix. In the initial step, we employed the HPP as well as both power-law and log-linear models to fit the TBE variable based on a RANHPP and chose the model based on the Akaike Information Criterion (AIC). Among them, the power-law model yielded a better fit. The estimated parameters are in Table 8 where $\hat{\beta}_1, \hat{\beta}_2, \hat{\beta}_3, \hat{\beta}_4$, and $\hat{\beta}_5$ are the regression coefficients of PL, PT, LT, AS, and CC, respectively. The hazard ratios (HR) defined as e^{β} regarding risk factors are also reported in this table. In this context, HR quantifies the multiplicative change in the hazard rate for a one-unit increase in the risk factor. In this way, HR > 1 (< 1) indicates an increase (decrease) in the hazard rate associated with a one-unit change in the risk factor. Furthermore, $HR = 1$ implies that there is no change in the hazard rate associated with a one-unit change in the predictor variable.

Based on the table, $\hat{\eta} > 1$ indicates that the hazard rate of the pipelines is increasing over time, which aligns with our expectation given their degradation nature. This translates to a higher frequency of failures or a shorter TBE in the presence of aging. Furthermore, the estimated coefficients of the risk model show that there is a negative association between the risk factors PL and the TBE variable ($\beta_1 < 0$ with corresponding HR < 1), whereas covariates PT, LT, AS, and CC are positively associated with TBE ($\beta_2 > 0, \beta_3 > 0, \beta_4 > 0$, and $\beta_5 > 0$ with corresponding HR > 1). Furthermore, according to the HR criteria, we can see that the risk factor PL (pipeline location) has the most effect on TBE compared to the other risk factors.

Now, turning to the TC variable denoted by Y. To assess the distribution of Y_i's, a Kolmogorov–Smirnov test with corresponding p-value = 0.025 suggests that an exponential distribution with mean $\frac{1}{\hat{\mu}} = 311,905$ USD could be a reasonable model for the TC variable. In the second step of our analysis, the focus shifts to selecting the most suitable copula based on the estimated parameters obtained in the first step. We search through three Archimedean copula functions, including Gumbel, Frank and Clayton, to find the most suitable model for describing the dependence structure between variables $X_i | T_{i-1}, \mathbf{z_i}$ and Y_i. Based on the AIC metric, the Gumbel copula with $\tau = 0.001$ is the optimal choice that indicates a weak positive dependence between the TBE and TC variables. Eventually, the estimated parameters in Table 8 can be used to establish the control limits of the proposed approach in Phase II to monitor the AC over time through the ratios $W_i = \frac{Y_i}{X_i}$ for $i = 1, 2, \dots$.

7.3 | Phase II Analysis

To calculate the control limits in this phase, we set $\mathrm{ARL}_0 = 200$ corresponding to the false alarm rate $\alpha = 0.005$. Figure 6a depicts

the control chart representing the last one hundred observations of W_i. Since the distribution of W_i is highly right-skewed, is hard to conclude the stability of the process from this figure. Thus, to better illustrate, Figure 6b shows the control chart after taking a logarithm of the monitor statistics and their corresponding control limits. The updated figure makes it much easier to assess the random behavior of W_i within the IC zoon and to highlight its OC observations. Figure 6b shows nine OC signals by plotting W_i below the LCL_i. For more illustration, Table 9 presents the information of the last 50 failures. The OC signals are shown by bold-red values in this table. Considering all this information, the proposed control chart suggests evidence of a potential decrease (improvement) in the AC parameter.

Although the control chart for AC provides valuable insights into the process, it does not address whether the TBE, the TC, or both of them have shifted. This is a known disadvantage of control charts based on more than characteristics. In such cases, one idea is to develop control charts for monitoring TBE and TC individually to find the main source of shift in the AC. Figure 6c,d show separate control charts for X_i and Y_i. Note that the control limits of TBE and TC charts are obtained based on the quantiles of the conditional CDF of X_i in (14) and the quantiles of the CDF of the exponential distribution, respectively. Figure 6d indicates that the TBE variable remains relatively stable statistically throughout this period. However, in panel (c), the control chart of TC displays several OC signals, particularly towards the end of the monitoring period. This coincides with the presence of OC signals on the AC chart (panel (a) of this figure). On the other hand, the TC's control chart shows a downward shift in Y_i, which is the same as the direction of AC's shift. By analyzing the insights provided by both the joint and individual control charts, it can be concluded that the downward deviation in TC is the root cause of the observed OC condition in the AC's control chart.

It is important to note that while a downward shift in AC/TC is a positive sign, the inspectors should continue the monitoring process for some time to ensure that the improvement is sustained and that other aspects of the process are not adversely affected. Since the TC is the aggregate sum of all incurred costs, the manager can investigate what specific cost factor(s) have contributed to the decrease in TC. In case a sustained decrease in TC is approved, the quality inspector should plan to collect data and reestablish control limits based on new data.

8 | Conclusion

This article introduced a risk-adjusted control chart to simultaneously monitor the time between and the cost associated with consecutive failures of systems. This is done by monitoring the ratio of the TC and the TBE variables based on an NHPP model. The inclusion of risk adjustment serves to account for risk factors that improve the chart's sensitivity to variations in process failure and cost. The TBE and TC variables are assumed to be dependent such that a copula model can describe their dependency. The effectiveness of the proposed methods is assessed using the ARL and SDRL metrics. Extensive simulations have been conducted to evaluate the performance of the control chart with respect to the various process parameters. In general, there are three categories of parameters, the parameters corresponding to the TBE (γ and

TABLE 9 | The information on the last 50 accidents.

i	T_i	X_i	Y_i	W_i	LCL_i	UCL_i	Z_{1i}	Z_{2i}	Z_{3i}	Z_{4i}	Z_{5i}
2732	59562.4	75.2	4575	60.8	36.9	13197434.0	ONS	ABG	CRO	OH	MWE
2733	59565.4	3.0	46280	15341.4	37.0	13168685.0	ONS	UNG	HFT	IL	MWE
2734	59583.8	18.4	73569	3998.3	37.1	13132831.0	ONS	ABG	RPL	CA	MWE
2735	59584.2	0.5	3571	7652.1	36.3	13439985.0	ONS	ABG	CRO	KS	MWE
2736	59586.3	2.1	4020	1961.0	38.1	12772968.0	ONS	UNG	HFT	TX	MWE
2737	59652.9	66.7	5011	75.2	36.6	13330405.0	ONS	TAN	RPL	NJ	AOC
2738	59684.6	31.7	2336	73.7	38.5	12624830.0	ONS	TAN	RPL	SD	MWE
2739	59695.9	11.3	60000	5301.9	37.3	13084386.0	ONS	ABG	CRO	TX	MWE
2740	59712.1	16.2	157221	9725.0	36.7	13303158.0	ONS	ABG	CO2	TX	MWE
2741	59769.9	57.8	4120	71.3	36.4	13410679.0	ONS	UNG	CRO	TX	COR
2742	59871.1	101.2	4521	44.7	37.3	13081148.0	ONS	ABG	CRO	TX	MWE
2743	59892.1	21.1	5417	257.3	37.9	12853827.0	ONS	ABG	HFT	TX	MWE
2744	59894.7	2.6	145310	56249.0	35.1	13876192.0	ONS	UNG	CRO	CA	COR
2745	59903.1	8.4	1016236	121462.5	35.9	13564725.0	ONS	UNG	HFT	MO	AOC
2746	59914.1	11.1	3089580	279600.0	37.6	12966895.0	ONS	ABG	RPL	LA	MWE
2747	59936	21.9	157000	7174.4	38.5	12619194.0	ONS	ABG	RPL	TX	MWE
2748	59936.6	0.6	22203	39181.8	35.3	13810797.0	ONS	ABG	CO2	UT	AOC
2749	59943.4	6.9	70015	10171.7	37.3	13079746.0	ONS	ABG	CRO	TX	MWE
2750	59962.4	19.0	825	43.5	37.1	13133272.0	ONS	ABG	RPL	AR	MWE
2751	59963.1	0.7	800	1142.9	38.0	12795613.0	ONS	TRA	CRO	WY	NFD
2752	59971.9	8.8	400	45.5	36.2	13460802.0	ONS	ABG	CRO	IL	MWE
2753	60039.1	67.2	7500	111.6	35.5	13721322.0	ONS	UNG	CRO	ND	AOC
2754	60070.2	31.1	45	**1.4**	36.9	13216967.0	ONS	ABG	CRO	TX	INO
2755	60081.7	11.5	100500	8713.9	37.8	12894699.0	ONS	ABG	HFT	SC	MWE
2756	60143.9	62.1	523	8.4	37.2	13105401.0	ONS	UNG	RPL	TX	AOC
2757	60168.1	24.3	1820500	75072.2	38.1	12763518.0	ONS	ABG	RPL	TX	INO
2758	60171.1	3.0	1000	339.0	37.5	13006054.0	ONS	ABG	HFT	NM	MWE
2759	60173.9	2.8	27580	9850.0	38.1	12761980.0	ONS	ABG	RPL	TX	INO
2760	60212.8	38.9	43	**1.1**	37.5	12990762.0	ONS	ABG	HFT	TX	INO
2761	60230.4	17.7	20200	1143.4	37.9	12847206.0	ONS	ABG	HFT	TX	MWE
2762	60244.8	14.4	30400	2111.1	38.0	12789663.0	ONS	UNG	RPL	VA	EXD
2763	60252.6	7.8	15000	1931.3	36.9	13214086.0	ONS	ABG	CRO	TX	INO
2764	60259.7	7.1	6400	903.5	36.0	13536355.0	ONS	UNG	CRO	TX	AOC
2765	60281.8	22.1	119829	5418.0	38.6	12554030.0	ONS	TAN	RPL	OH	NFD
2766	60322.6	40.8	9450	231.6	36.9	13211372.0	ONS	TAN	CRO	NJ	MWE
2767	60371.4	48.8	1050	**21.5**	37.3	13073569.0	ONS	ABG	CRO	TX	MWE
2768	60378.4	7.1	375	52.9	37.7	12931277.0	ONS	ABG	CRO	TX	NFD
2769	60378.8	0.3	100	300.0	35.8	13625136.0	ONS	UNG	CRO	OK	AOC
2770	60379.4	0.6	10993	18845.1	36.4	13399666.0	ONS	ABG	CRO	LA	MWE
2771	60404.9	25.5	7803	306.0	35.8	13625152.0	ONS	UNG	CRO	OK	AOC
2772	60424.3	19.4	300	**15.5**	36.3	13439608.0	ONS	ABG	CRO	IN	MWE
2773	60458.0	33.8	227	**6.7**	36.6	13319821.0	ONS	ABG	CRO	MO	MWE
2774	60475.6	17.6	5000	284.4	35.8	13607860.0	ONS	ABG	CRO	TX	AOC
2775	60494.2	18.6	2600	139.9	37.3	13070748.0	ONS	ABG	CRO	TX	MWE

(Continues)

TABLE 9 | (Continued)

i	T_i	X_i	Y_i	W_i	LCL_i	UCL_i	Z_{1i}	Z_{2i}	Z_{3i}	Z_{4i}	Z_{5i}
2776	60539.9	45.8	906900	19823.0	36.2	13479949.0	ONS	ABG	CRO	TX	COR
2777	60565.3	25.3	26315	1038.8	36.6	13318231.0	ONS	ABG	CRO	MO	MWE
2778	60596.9	31.7	17456	551.2	35.8	13634449.0	ONS	UNG	HFT	LA	AOC
2779	60611.3	14.3	170	**11.9**	37.1	13134282.0	ONS	TAN	CRO	OK	MWE
2780	60734.6	123.3	20333	164.9	37.0	13166475.0	ONS	UNG	RPL	PA	AOC
2781	60876.3	141.7	165593	1168.9	36.9	13205625.0	ONS	ABG	CRO	TX	INO

η) and TC (μ) variables, the vector of coefficients $\boldsymbol{\beta}$ associated with the risk model, and the parameter of the copula model θ_c. During the simulation study, we only focused on assessing the performance of the proposed technique in monitoring γ, η and μ. In summary, the numerical study yields the following insights:

- The proposed chart is ARL-unbiased across all shift combinations, i.e., we always have $ARL_0 > ARL_1$.

- A higher degree of dependency between TBE and TC improves the chart's ability to detect shifts sooner.

- The risk factors exhibiting a negative association with TBE have a positive impact on the performance of the proposed chart, while those with a positive association negatively impact the efficiency of the monitoring technique.

- Risk factors can notably increase the false alarm rate if not accounted for properly in the design of the chart.

The last two bullet points underscore the critical importance of incorporating risk adjustment to improve the effectiveness of the proposed control chart. By accounting for the risk factors, the chart's detection capability is enhanced through the isolation of the underlying failure mechanism, achieved via separate estimation of the effects associated with those risk factors. Furthermore, the superiority of the proposed approach over existing methods that disregard such factors has been demonstrated through comparative numerical simulations, reinforcing its practical value in real-world monitoring applications.

To implement the proposed method effectively, several model parameters must be estimated from a clean (in-control or reference) data set. Prior studies have shown that parameter estimation errors can significantly affect the performance of control charts. Therefore, evaluating the impact of estimation errors in Phase I on the monitoring performance in Phase II presents a valuable direction for future research. Additionally, although our proposed chart incorporates the TC associated with failures in its monitoring statistic, the design is based purely on statistical considerations, such as in-control and out-of-control performance metrics. In practice, however, failure events often involve various tangible costs. Although these were included in the original version of the dataset analyzed in Section 7, they were not reported in this study and include property damage, emergency response, and environmental remediation costs. Integrating such cost components into the design of the control chart could help achieve not only desirable statistical properties but also minimize financial loss. Thus, an economic-

statistical design of the proposed methodology represents another promising and practically relevant avenue for future research.

Data Availability Statement

The data that support the findings of this study are available in Oil Pipeline Accidents, 2010-Present at https://www.kaggle.com/datasets/usdot/pipeline-accidents. These data were derived from the following resources available in the public domain: - Kaggle, https://www.kaggle.com/datasets/usdot/pipeline-accidents.

References

1. D. C. Montgomery, *Introduction to Statistical Quality Control* (John Wiley & sons, 2019).

2. L. You and P. Qiu, "An Effective Method for Online Disease Risk Monitoring," *Technometrics* 62, no. 2 (2020): 249–264.

3. N. T. Stevens, J. D. Wilson, and A. R. Driscoll, "Research in Network Monitoring: Connections With SPM and New Directions," *Quality Engineering* 33, no. 4 (2021): 736–748.

4. K. Bisiotis, S. Psarakis, and A. N. Yannacopoulos, "Control Charts in Financial Applications: An Overview," *Quality and Reliability Engineering International* 38, no. 3 (2022): 1441–1462.

5. P. Qiu and X. Xie, "Transparent Sequential Learning for Statistical Process Control of Serially Correlated Data," *Technometrics* 64, no. 4 (2022): 487–501.

6. H. Wu, Q. Liang, and K. Wang, "Modeling and Monitoring Multilayer Attributed Weighted Directed Networks via a Generative Model," *IISE Transactions* 56, no. 8 (2024): 902–914.

7. A. Miraliakbar and Z. Jiang, "Fast, Accurate, and Robust Fault Detection and Diagnosis of Industrial Processes," *Systems and Control Transactions* 3 (2024): 322–329.

8. A. Miraliakbar, F. Ma, and Z. Jiang, "Online Fault Detection and Classification of Chemical Process Systems Leveraging Statistical Process Control and Riemannian Geometric Analysis," *Computers & Chemical Engineering* 200 (2025): 109177.

9. M. Kovarik, L. Sarga, and P. Klímek, "Usage of Control Charts for Time Series Analysis in Financial Management," *Journal of Business Economics and Management* 16, no. 1 (2015): 138–158.

10. H. Ahmad, A. A. Nadi, M. Amini, and B. S. Gildeh, "Monitoring Processes With Multiple Dependent Production Lines Using Time Between Events Control Charts," *Quality Engineering* 35, no. 4 (2023): 639–668.

11. H. Ahmad, M. Amini, B. S. Gildeh, and A. A. Nadi, "Copula-Based Multivariate EWMA Control Charts for Monitoring the Mean Vector of Bivariate Processes Using a Mixture Model," *Communications in Statistics-Theory and Methods* 53 (2023): 1–24.

12. P. Castagliola, G. Celano, D. Rahali, and S. Wu, "Control Charts for Monitoring Time-Between-Events-and-Amplitude Data," in *Control Charts and Machine Learning for Anomaly Detection in Manufacturing* (Springer International Publishing, 2021) 43–76.

13. N. Kumar, S. Chakraborti, and P. Castagliola, "Phase II Exponential Charts for Monitoring Time Between Events Data: Performance Analysis Using Exact Conditional Average Time to Signal Distribution," *Journal of Statistical Computation and Simulation* 92, no. 7 (2022): 1457–1486.

14. N. G. Dincer, S. Demir, and M. O. Yalçin, "Forecasting COVID19 Reliability of the Countries by Using non-Homogeneous Poisson Process Models," *New Generation Computing* 40, no. 4 (2022): 1143–1164.

15. Y. Hong and W. Q. Meeker, "Comments on 'Virtual Age, is it Real?(Discussing Virtual age in Reliability Context)' by M. Finkelstein and J. H. Cha," *Applied Stochastic Models in Business and Industry* 37, no. 1 (2021): 32–34.

16. V. Pradhan, A. Kumar, and J. Dhar, "Enhanced Growth Model of Software Reliability With Generalized Inflection S-Shaped Testing-Effort Function," *Journal of Interdisciplinary Mathematics* 25, no. 1 (2022): 137–153.

17. J. H. Cha and M. Finkelstein, *Point Processes for Reliability Analysis: Shocks and Repairable Systems*, 1st ed. (Springer International Publishing 2018).

18. F. Safaei, J. Ahmadi, and N. Balakrishnan, "A Repair and Replacement Policy for Repairable Systems Based on Probability and Mean of Profits," *Reliability Engineering & System Safety* 183 (2019): 143–152.

19. T. Yuan, T. Yan, and S. J. Bae, "Superposed Poisson Process Models With a Modified Bathtub Intensity Function for Repairable Systems," *IISE Transactions* 53, no. 9 (2021): 1037–1051.

20. F. Safaei and S. Taghipour, "Optimal Preventive Maintenance for Repairable Products With Three Types of Failures Sold Under a Renewable Hybrid FRW/PRW Policy," *Reliability Engineering & System Safety* 223 (2022): 108392.

21. Z. Xu, Y. Hong, W. Q. Meeker, B. E. Osborn, and K. Illouz, "A Multi-Level Trend-Renewal Process for Modeling Systems With Recurrence Data," *Technometrics* 59, no. 2 (2017): 225–236.

22. L. Qu, S. He, M. B. Khoo, and P. Castagliola, "A CUSUM Chart for Detecting the Intensity Ratio of Negative Events," *International Journal of Production Research* 56, no. 19 (2018): 6553–6567.

23. D. Rahali, P. Castagliola, H. Taleb, and M. B. Khoo, "Evaluation of Shewhart Time-Between-Events-and-Amplitude Control Charts for Several Distributions," *Quality Engineering* 31, no. 2 (2019): 240–254.

24. R. A. Sanusi, S. Y. Teh, and M. B. Khoo, "Simultaneous Monitoring of Magnitude and Time-Between-Events Data With a Max-EWMA Control Chart," *Computers & Industrial Engineering* 142 (2020): 106378.

25. S. Zhang, Q. Zhai, and Y. Li, "Degradation Modeling and RUL Prediction With Wiener Process Considering Measurable and Unobservable External Impacts," *Reliability Engineering and System Safety* 231 (2023): 109021.

26. H. Zheng, X. Kong, H. Xu, and J. Yang, "Reliability Analysis of Products Based on Proportional Hazard Model With Degradation Trend and Environmental Factor," *Reliability Engineering & System Safety* 216 (2021): 107964.

27. S. H. Steiner and M. Jones, "Risk - Adjusted Survival Time Monitoring With an Updating Exponentially Weighted Moving Average (EWMA) Control Chart," *Statistics in Medicine* 29, no. 4 (2010): 444–454.

28. M. Cockeran, S. G. Meintanis, and J. S. Allison, "Goodness-of-fit Tests in the Cox Proportional Hazards Model," *Communications in Statistics-Simulation and Computation* 50, no. 12 (2021): 4132–4143.

29. S. H. Steiner, R. J. Cook, and V. T. Farewell, "Risk-Adjusted Monitoring of Binary Surgical Outcomes," *Medical Decision Making* 21, no. 3 (2001): 163–169.

30. S. H. Steiner, R. J. Cook, V. T. Farewell, and T. Treasure, "Monitoring Surgical Performance Using Risk-Adjusted Cumulative Sum Charts," *Biostatistics* 1, no. 4 (2000): 441–452.

31. A. Sachlas, S. Bersimis, and S. Psarakis, "Risk-Adjusted Control Charts: Theory, Methods, and Applications in Health," *Statistics in Biosciences* 11 (2019): 630–658.

32. S. H. Steiner and R. J. Mackay, "Monitoring Risk-Adjusted Medical Outcomes Allowing for Changes Over Time," *Biostatistics* 15, no. 4 (2014): 665–676.

33. W. H. Woodall, S. L. Fogel, and S. H. Steiner, "The Monitoring and Improvement of Surgical-Outcome Quality," *Journal of Quality Technology* 47, no. 4 (2015): 383–399.

34. K. Paynabar, J. Jin, and A. B. Yeh, "Phase I Risk-Adjusted Control Charts for Monitoring Surgical Performance by Considering Categorical Covariates," *Journal of Quality Technology* 44, no. 1 (2012): 39–53.

35. S. H. Steiner, "Risk-Adjusted Monitoring of Outcomes in Health Care," *Statistics in Action: A Canadian Outlook* 14 (2014): 225–241.

36. B. M. Mun, P. H. Kvam, and S. J. Bae, "Mixed-Effects Nonhomogeneous Poisson Process Model for Multiple Repairable Systems," *IEEE Access* 9 (2021): 71900–71908.

37. X. Y. Tian, X. Shi, C. Peng, and X. J. Yi, "A Reliability Growth Process Model With Time-Varying Covariates and its Application," *Mathematics* 9, no. 8 (2021): 905.

38. P. Li, Q. Cai, W. Lin, B. Chen, and B. Zhang, "Offshore Oil Spill Response Practices and Emerging Challenges," *Marine Pollution Bulletin* 110, no. 1 (2016): 6–27.

39. H. Lu, D. Xi, and G. Qin, "Environmental Risk of Oil Pipeline Accidents," *Science of the Total Environment* 874 (2023): 162386.

40. Z. Wang and S. Stout, *Oil Spill Environmental Forensics: Fingerprinting and Source Identification* (Elsevier, 2010).

41. D. Xi, H. Lu, Y. Fu, S. Dong, X. Jiang, and J. Matthews, "Carbon Dioxide Pipelines: A Statistical Analysis of Historical Accidents," *Journal of Loss Prevention in the Process Industries* (2023): 105129.

42. I. C. White and F. C. Molloy, "Factors That Determine the Cost of Oil Spills," *International Oil Spill Conference* 2003, no. 1 (April 2003): 1225–1229.

43. D. S. Etkin, "Modeling Oil Spill Response and Damage Costs," in *Proceedings of the Fifth Biennial Freshwater Spills Symposium*, vol. 15, (U.S. Environmental Protection Agency, 2004).

44. M. M. Cobanoglu, S. Kermanshachi, and I. Damnjanovic, "Statistical Modeling of Corrosion Failures in Natural Gas Transmission Pipelines," *Pipelines* 2016 (2016): 195–204.

45. S. Kermanshachi, B. Rouhanizadeh, M. M. Cobanoglu, and I. Damnjanovic, "Optimal Pipeline Maintenance Strategies in the United States: Stochastic Reliability Analysis of Gas Pipeline Network Failures," *Journal of Pipeline Systems Engineering and Practice* 11, no. 1 (2020): 04019041.

46. H. Hofmann, H. Wickham, and K. Kafadar, "Value Plots: Boxplots for Large Data," *Journal of Computational and Graphical Statistics* 26, no. 3 (2017): 469–477.

47. R. B. Nelsen, *An Introduction to Copulas* (Springer, 2006).

48. M. Emile and J. Gumbel, "Distributions des Valeurs Extrêmes en Plusieurs Dimensions," *Annales de l'ISUP* 9, no. 2 (1960): 171–173.

49. S. Chakraborti and M. Graham, *Nonparametric Statistical Process Control* (John Wiley & Sons, 2019).

50. S. Ali, "Time-Between-Events Monitoring Using Nonhomogeneous Poisson Process With Power Law Intensity," *Quality and Reliability Engineering International* 37, no. 8 (2021): 3157–3178.

Appendix A: Estimation method

This section offers the required methodology to estimate the parameters of the model. Consider the continuous TBE and TC random variables, denoted as X_i and Y_i so that their joint distribution function is described by the copula function C. The joint PDF of TBE and TC is given in (17). Then, the likelihood function to estimate the unknown vectors θ_X, θ_Y, and θ_c can be calculated based on the paired observations $(x_i, y_i)_{i=1,\dots,n}$ as:

$$
\ell\left(\theta_X, \theta_Y, \theta_c | (x_i, y_i)_{i=1,\dots,n}\right)
$$
$$
= \sum_{i=1}^{n} \ln c\left(F_{(X_i | t_{i-1}, z_i)}(x_i | \theta_X), F_Y(y_i | \theta_Y) | \theta_c\right)
$$
$$
+ \sum_{i=1}^{n} \ln f_{(X_i | t_{i-1}, z_i)}(x_i | \theta_X) + \sum_{i=1}^{n} \ln f_Y(y_i | \theta_Y), \quad (A.1)
$$

where c is copula pdf. When dealing with multivariate models, it's common to encounter situations where closed-form estimators, such as maximum likelihood or other analytical methods, are not readily available. In such cases, numerical techniques become essential. Moreover, as the dimensionality of the problem increases, the challenges associated with numerical optimization become more pronounced, especially in the presence of a copula function. In light of these complexities, Joe and Xu (1996) proposed an approach called inference function for margins (IFM) which is particularly useful when we have data from multiple variables and we want to model their joint distribution using copulas. Joe and Xu (1996) showed that the IFM approach has some benefits over the traditional maximum likelihood estimation (MLE) method; it tends to be computationally simpler compared to MLE, especially for complex copula models and it can be more robust to misspecification of the marginal distributions. Even if the marginal models are not perfectly specified, the IFM approach can still provide reliable estimates of the copula parameters. In the current setting, one may encounter a problem with tens of risk factors, potentially significantly increasing the dimension of the parameter space. Therefore, we adopt the IFM approach to estimate the parameters. According to this approach, we apply the following two steps in the estimation procedure.

1. Estimate the parameters of the margins θ_X and θ_Y as:

$$
\hat{\theta}_Y = \arg\max \ell_Y\left(\hat{\theta}_Y | (y_i)_{i=1,\dots,n}\right), \quad (A.2)
$$

$$
\hat{\theta}_X = \arg\max \ell_X\left(\theta_X | (x_i)_{i=1,\dots,n}\right), \quad (A.3)
$$

where ℓ_Y and ℓ_X are the log-likelihood functions based Y_i and $X_i | (t_{i-1}, z_i)$ for $i = 1, 2, \dots, n$, respectively. If Y_i follows an Exponential distribution, like the case study, we have $\hat{\theta}_Y = \mu$ and:

$$
\hat{\mu} = \frac{n}{\sum_{i=1}^{n} y_i} \quad (A.4)
$$

2. Given $\hat{\theta}_X$ and $\hat{\theta}_Y$ obtained in step 1, estimate the copula parameter θ_c as:

$$
\hat{\theta}_c = \arg\max \ell_c\left(\theta_c, \hat{\theta}_X, \hat{\theta}_Y | (x_i, y_i)_{i=1,\dots,n}\right), \quad (A.5)
$$

where ℓ_c is the copula log-likelihood function.

To estimate the parameters using (A.3), the Equation (15) will be used to determined the log-likelihood function as:

$$
\ell_X(\theta_X | x_1, x_2, \dots, x_n)
$$

$$
= \sum_{i=1}^{n} log(\lambda(t_{i-1} + x_i | z_i)) - \sum_{i=1}^{n} [\Lambda(t_{i-1} + x_i | z_i) - \Lambda(t_{i-1} | z_i)]
$$

$$
= \sum_{i=1}^{n} log(\lambda(t_{i-1} + x_i) \exp(\beta' z_i)) - \sum_{i=1}^{n} [\Lambda(t_{i-1} + x_i) - \Lambda(t_{i-1})] \exp(\beta' z_i)
$$

$$
= \sum_{i=1}^{n} log(\lambda(t_{i-1} + x_i)) + \sum_{i=1}^{n} (\beta' z_i) - \sum_{i=1}^{n} [\Lambda(t_{i-1} + x_i) - \Lambda(t_{i-1})] \exp(\beta' z_i). \quad (A.6)
$$

Accordingly, if we consider the power law intensity, then (A.6) reduces to:

$$
\ell_X(\beta', \gamma, \eta | x_1, x_2, \dots, x_n)
$$

$$
= \sum_{i=1}^{n} log(\gamma\eta(t_{i-1} + x_i)^{\eta-1}) + \sum_{i=1}^{n} (\beta' z_i)
$$

$$
- \sum_{i=1}^{n} \gamma\left((t_{i-1} + x_i)^{\eta} - t_{i-1}^{\eta}\right) \exp(\beta' z_i)
$$

$$
= n log(\gamma) + n log(\eta) + (\eta - 1) \sum_{i=1}^{n} log(t_{i-1} + x_i)
$$

$$
+ \sum_{i=1}^{n} (\beta' z_i) - \sum_{i=1}^{n} \gamma[(t_{i-1} + x_i)^{\eta} - t_{i-1}^{\eta}] \exp(\beta' z_i) \quad (A.7)
$$

In the same way, in the case of the Log-Linear intensity, (A.6) reduces to:

$$
\ell_X(\beta', \gamma, \eta | x_1, x_2, \dots, x_n)
$$

$$
= \sum_{i=1}^{n} log(exp(\gamma + \eta(t_{i-1} + x_i))) + \sum_{i=1}^{n} (\beta' z_i)
$$

$$
- \sum_{i=1}^{n} \frac{1}{\eta}(exp(\gamma + \eta(t_{i-1} + x_i)) - exp(\gamma + \eta t_{i-1})) \exp(\beta' z_i)
$$

$$
= n\gamma + \eta \sum_{i=1}^{n} (t_{i-1} + x_i) + \sum_{i=1}^{n} (\beta' z_i)
$$

$$
- \frac{exp(\gamma)}{\eta} \sum_{i=1}^{n} [\exp(\eta(t_{i-1} + x_i)) - exp(\eta t_{i-1})] \exp(\beta' z_i). \quad (A.8)
$$

Eventually, $\hat{\theta}_X$ can be obtained in both scenarios by substituting (A.7) and (A.8) in (A.3) and solving the optimization problem.